

JAN 23 1953

~~SECRET~~

UNCLASSIFIED

RM L52K26

C. 2

NACA RM L52K26



RESEARCH MEMORANDUM

THE LOW-SPEED LIFT AND PITCHING-MOMENT
CHARACTERISTICS OF A 45° SWEEPBACK WING OF ASPECT RATIO 8
WITH AND WITHOUT HIGH-LIFT AND STALL-CONTROL DEVICES AS
DETERMINED FROM PRESSURE DISTRIBUTIONS AT
A REYNOLDS NUMBER OF 4.0×10^6

By Thomas V. Bollech and William M. Hadaway

Aeronautical Laboratory
Langley Field, Va.

CLASSIFICATION CANCELLED

Authority J. A. Crowley Date 12/7/53
(E.O. 10569)
By DATA 12/18/53 See NACA
R 7 1665

CLASSIFIED DOCUMENT

This material contains information affecting the National Defense of the United States within the meaning of the espionage laws, Title 18, U.S.C., Secs. 793 and 794, the transmission or revelation of which in any manner to an unauthorized person is prohibited by law.

NATIONAL ADVISORY COMMITTEE FOR AERONAUTICS

WASHINGTON
January 20, 1953

UNCLASSIFIED

NACA LIBRARY
NATIONAL AERONAUTICAL LABORATORY
Langley Field, Va.

~~SECRET~~



NATIONAL ADVISORY COMMITTEE FOR AERONAUTICS

RESEARCH MEMORANDUM

THE LOW-SPEED LIFT AND PITCHING-MOMENT
CHARACTERISTICS OF A 45° SWEEPBACK WING OF ASPECT RATIO 8
WITH AND WITHOUT HIGH-LIFT AND STALL-CONTROL DEVICES AS
DETERMINED FROM PRESSURE DISTRIBUTIONS AT
A REYNOLDS NUMBER OF 4.0×10^6

By Thomas V. Bollech and William M. Hadaway

SUMMARY

The manner in which the lift and pitching-moment characteristics of a 45° sweptback wing are influenced by high-lift and stall-control devices was determined from detailed pressure-distribution measurements. The wing had an aspect ratio of 8, a taper ratio of 0.45, and incorporated NACA 63₁A012 airfoil sections. It was equipped with extended and split trailing-edge flaps, extensible leading-edge flaps, and upper-surface fences. The investigation was conducted in the Langley 19-foot pressure tunnel at a Reynolds number of 4.0×10^6 and a Mach number of 0.19.

Although it was not positively established, the results indicate that the instability of the basic wing, which began to occur at a lift coefficient of approximately 0.25, was due to flow separation which originated over the outer 4 percent of the wing semispan.

The stability of the wing in the upper portion of the lift-coefficient range was improved through the use of upper-surface fences or leading-edge flaps.

The increased lift effectiveness of the extended trailing-edge flaps was due to the increased chord of the sections spanned by the flaps rather than to an increase in the individual pressures acting on sections.

INTRODUCTION

As a result of considerable research effort, the low-speed stability and lift characteristics of swept wings have been improved through the use of leading- and trailing-edge flaps and upper-surface fences. Although considerable force test data are available which show the over-all effects of varying spans of leading- and trailing-edge flaps and various types of upper-surface fences on the low-speed characteristics of swept wings, only a limited amount of pressure-distribution data are available to show the effects of the various devices on the chordwise and spanwise load distributions.

A pressure-distribution investigation, therefore, was carried out in the Langley 19-foot pressure tunnel on a 45° sweptback wing of aspect ratio 8 with and without high-lift and stall-control devices to aid in the further study of the effects of these devices on the lift and pitching-moment characteristics of swept wings. The high-lift and stall-control devices consisted of split and extended trailing-edge flaps, round-nose extensible leading-edge flaps, and upper-surface fences.

The investigation was carried out through an angle-of-attack range from -4° through the stall at a Reynolds number of 4.0×10^6 and a Mach number of 0.19.

An analysis of the longitudinal characteristics of the subject wing as determined from force data of the wing with and without high-lift and stall-control devices has been presented in reference 1. The present paper concerning the longitudinal characteristics of the subject wing employs the results of the pressure distribution tests as an aid in analyzing the flow characteristics of the wing that produced the force-data trends obtained.

SYMBOLS

The data are referred to the wind axes with the origin of these axes located at the projection of the quarter-chord point of the mean aerodynamic chord on the plane of symmetry and have been reduced to nondimensional coefficients which are defined as follows:

$$C_L \quad \text{lift coefficient, } \frac{L}{qS} \text{ or } \int_0^1 c_l \frac{c}{c} d \frac{y}{b/2}$$

$$c_l \quad \text{section lift coefficient,}$$

$$\cos \alpha \int_0^1 (P_l - P_u) d \frac{x}{c} - \sin \alpha \int_{-(z/c)_{\max}}^{(z/c)_{\max}} (P_f - P_r) d \frac{z}{c}$$

C_m	pitching-moment coefficient, $\frac{M}{qSc'}$
$c_{m_c} / 4$	section pitching-moment coefficient, $c_m - \frac{x_c/4}{c} \int_0^1 (P_l - P_u) d \frac{x}{c}$
C_m	section pitching-moment coefficient about the local quarter chord, $\int_0^1 (P_l - P_u) \left(0.25 - \frac{x}{c}\right) d \frac{x}{c} + \int_{-(z/c)_{\max}}^{(z/c)_{\max}} (P_f - P_r) \frac{z}{c} d \frac{z}{c}$
$\frac{dC_L}{d\alpha}$	rate of change of lift coefficient with angle of attack
$\frac{dC_m}{d\alpha}$	rate of change of pitching moment with angle of attack
α	angle of attack
L	lift
M	pitching moment about $0.25c'$
S	wing area
c'	mean aerodynamic chord, $\frac{2}{S} \int_0^{b/2} c^2 dy$
\bar{c}	mean geometric chord, $\frac{S}{b}$
c	local wing chord parallel to the plane of symmetry
b	wing span
q	dynamic pressure, $\rho V^2 / 2$
V	free-stream velocity
ρ	density of air
P	pressure coefficient, $\frac{P - P_0}{q}$

P_0	free-stream static pressure
P	local static pressure
x	longitudinal distance from local leading edge measured along chord plane and parallel to plane of symmetry (rearward positive)
$x_c/4$	longitudinal distance from quarter chord of c' to local quarter chord (rearward positive)
y	lateral distance from plane of symmetry measured perpendicular to plane of symmetry
z	vertical distance from chord plane measured perpendicular to chord plane (upward positive)
\bar{x}	longitudinal distance from quarter chord of c' to centroid of normal force (chordwise center of pressure, rearward positive)

Subscripts:

u	upper surface
l	lower surface
f	forward of maximum thickness
r	rearward of maximum thickness

MODEL

A layout of the model used in the investigation is presented as figure 1. The wing incorporated 45° of sweepback of the quarter-chord line, an aspect ratio of 8.02, a taper ratio of 0.45, and NACA 63₁A012 airfoil sections parallel to the plane of symmetry. The wing was constructed of a steel core with a surface of bismuth and tin alloy. The wing tips were parabolic in plan form and cross section and extended over the outer 2.5 percent of the wing semispan. The wing had no geometric dihedral or twist. The wing was fitted with 203 pressure orifices which were distributed among seven spanwise stations, namely, 0-, 0.1-, 0.3-, 0.55-, 0.75-, 0.90-, and 0.96-percent of the semispan. The chordwise distribution of the orifices on the wing is shown in figure 1(a). Tubes were connected to the orifices and brought out of the model from the lower

surface of the right semispan through a pressure-tube transfer boom located approximately 20 percent of the semispan from the plane of symmetry (fig. 2). The tubes were then conducted to multitube manometers.

The high-lift and stall-control devices (fig. 1(b)) consisted of two types of split trailing-edge flaps, extensible round-nose leading-edge flaps and upper-surface fences.

The trailing-edge flaps were constructed of $\frac{1}{16}$ -inch sheet steel and had chords equal to 20 percent of the local wing chord parallel to the plane of symmetry in the undeflected position. The flaps were deflected 50° measured from the wing lower surface in the streamwise direction which corresponds to 60° measured perpendicular to the hinge line. The flap mounting brackets were constructed so that the hinge line could be located at 80 percent and 100 percent of the local chord. Hereafter, the flaps with their hinge lines located at 80 and 100 percent of the chord will be referred to as split and extended trailing-edge flaps, respectively (fig. 1(b)).

The extensible round-nose leading-edge flaps were fabricated of wood and a sheet-steel leading edge which was contoured to the dimensions given in figure 1(b). The flaps were deflected 30° from the wing-chord plane in the streamwise direction and had a constant chord of 2.817 inches which corresponds to 16 and 27 percent of the streamwise local wing chord at 40 and 97.5 percent of the wing semispan, respectively. Pressure orifices were installed in both trailing- and leading-edge flaps and were spaced spanwise to align with the spanwise orifice stations on the basic wing. The chordwise distribution of the orifices installed on the flaps is shown in figure 1(b).

The upper-surface fences are shown in figure 1(b) and correspond to the fence configuration referred to as chord fences in reference 1. The fences extended from 5 percent of the chord on the upper surface to the trailing edge of the wing and had a height equivalent to approximately 7 percent of the chord measured from the wing surface perpendicular to the wing-chord plane. The fences were constructed of $\frac{1}{16}$ -inch sheet steel and were located on the wing at 0.58 and 0.80 percent of the wing semispan.

TESTS

The tests were conducted in the Langley 19-foot pressure tunnel with the model installed in the test section as shown in figure 2. The air in the tunnel was compressed to approximately 33 pounds per square inch, absolute.

The pressure-distribution and force measurements were made through an angle-of-attack range from -4° through the stall at a Reynolds number of 4.0×10^6 and a Mach number of 0.19. The pressures indicated on the manometers were photographically recorded during the pressure-distribution tests. The force tests, measured with the standard six-component balance system, were made with the pressure-tube transfer boom removed. Results of a preliminary investigation indicated that the addition or removal of the transfer boom from the wing did not alter the aerodynamic characteristics of the wing.

CORRECTIONS TO DATA

The data obtained from force tests and pressure-distribution measurements have been corrected for air-stream misalignment (ref. 2). The force data also have been corrected for small support tare and interference effects. Inasmuch as the spanwise location of the orifice stations were judiciously selected to minimize or eliminate support interference, it can be assumed that the effects of tunnel supports on the chordwise pressure-distribution measurements are negligible. The angle of attack, drag, and pitching-moment coefficients obtained from force measurements have been corrected for jet-boundary effects in accordance with reference 3.

RESULTS AND DISCUSSION

Presentation of Data

The lift and pitching-moment characteristics as determined from force tests of the subject wing with and without high-lift and stall-control devices are presented in figures 3 and 4. The pitching-moment coefficients, lift coefficients, and center-of-pressure shifts for each chordwise wing section obtained in three-dimensional flow from pressure-distribution measurements are presented in figures 5 to 10. It should be noted that the values of section pitching moments have been weighted in accordance with their respective chord ratio, $c^2/\bar{c}c'$ so that a more realistic indication of the contribution of the various spanwise stations to the over-all wing pitching moment can be more readily ascertained.

The chordwise pressure distributions for the various model configurations are presented in figures 11 and 12. Figures 13 to 15 present the effects of leading-edge flaps of various span on the wing pitching-moment characteristics, chordwise pressure distributions, and span loading. The variations of the section lift coefficients and chordwise loading

with angle of attack for wing stations $\frac{2y}{b} = 0, 0.10, \text{ and } 0.30$ are shown in figure 16 and figures 17 and 18 present the span-load distributions of the wing with and without high-lift and stall-control devices. A comparison of the chordwise pressure distributions obtained on the inboard sections of the wing equipped with $0.45b/2$ leading-edge flaps and $0.5b/2$ split or extended trailing-edge flaps is presented in figure 19.

Effect of Leading-Edge Flaps and Fences on the
Longitudinal Stability Characteristics

Low-lift range ($C_L = 0$ to 0.3).-- An unstable trend occurs in the pitching-moment curve of the basic wing at a lift coefficient of approximately 0.25 which was not eliminated by the addition of upper-surface fences or leading-edge flaps but was somewhat delayed by the addition of $0.45b/2$ leading-edge flaps (fig. 3). Changes in slope of wing pitching-moment curves are usually associated with nonlinear lift changes and redistribution of lift. Figure 3 indicates that the wing $dC_L/d\alpha$ began to decrease at approximately $0.35C_L$, but the change in slope is not as well-defined as the change of dC_m/dC_L at approximately $0.25C_L$. An inspection of plain-wing section-lift values (fig. 7) indicates that section-lift-curve slopes are linear for all outboard sections to $\alpha \approx 5\frac{1}{2}^\circ$ corresponding to a C_L of 0.35. It is quite possible, however, that small nonlinear lift changes outboard of station $0.96b/2$ operating at a great distance from the wing moment center, as is the case for the subject high-aspect-ratio wing, could produce the initial unstable trend in the wing pitching-moment curve at $0.25C_L$. Another possibility might be that the chordwise center-of-pressure shifts along the span of the wing could produce the initial unstable pitching-moment trend without any nonlinear lift changes. This latter possibility apparently is not the case, however, since the variation of the chordwise centers of pressure (fig. 9) with lift coefficient is not of sufficient magnitude between a lift coefficient of 0.2 and 0.3 to account for the change in dC_m/dC_L . This condition is further substantiated by the linear variation of the section pitching-moment coefficient with wing lift coefficient (fig. 5) inasmuch as linear variations of section lift were obtained (fig. 7).

Although the pressure-distribution measurements are somewhat limited in the tip region by the number of pressure orifices that were installed at the wing tip, it would appear that the initial unstable trend in the pitching-moment curve of the basic wing is due to only very small changes in lift over the extreme part of the wing tips which have an influence

on the pitching-moment characteristics due to the high sweepback and large aspect ratio of the wing.

An estimate was made of the lift coefficient and the spanwise position at which initial flow separation would occur on the subject wing by the method of reference 4 which utilizes two-dimensional section data and simple sweep theory. The two-dimensional data were obtained from reference 5. The results of the calculations indicated that the initial flow separation should occur at 75 percent of the semispan at a lift coefficient of 0.55. Pressure-distribution data, however, indicated that the initial flow separation occurred at the wing tip at a lift coefficient of 0.35 or below. The discrepancy between the calculated and the experimental results is not unexpected, however, inasmuch as the method of reference 4 which utilizes two-dimensional data and simple sweep theory (ref. 6) apparently cannot adequately account for three-dimensional effects as, for example, the outward flow of boundary-layer air.

Moderate lift range ($C_L = 0.30$ to 0.95) -- In the moderate lift range the instability of the basic wing became more severe and was accompanied by a significant decrease in lift-curve slope (fig. 3). Both of these effects resulted from outward drainage of the boundary-layer air which caused flow separation at the trailing edge of the outboard sections of the wing which spread progressively inboard and forward with lift coefficient (fig. 11).

The addition of upper-surface fences alleviated trailing-edge flow separation (figs. 7 and 11) and materially reduced the instability through the moderate lift range previously noted for the basic wing (fig. 3). The fact that upper-surface fences resulted in a considerable delay in flow separation at the tip sections leads to the conclusion that, on the subject wing, the initial flow separation can be considered premature and due to the adverse effects of boundary-layer outflow.

Although 0.45b/2 leading-edge flaps did not eliminate trailing-edge separation over the outboard wing sections, they imparted camber to those sections and thereby increased and extended the section maximum lift coefficients to higher angles of attack (fig. 7(b)). A considerable quantity of lift was carried over the forward part of the outboard sections above a wing lift coefficient of approximately 0.7 (fig. 11); therefore, the pitching-moment contributions of the outboard sections were more favorable than those obtained for the basic wing (fig. 5). The fact that trailing-edge separation did occur over the outboard sections of the wing equipped with leading-edge flaps was probably influential in causing leading-edge flaps to be less effective from the standpoint of stability than upper-surface fences in the moderate lift range from a lift coefficient of 0.50 to 0.95. Although the vortex that is generated at the inboard end of the leading-edge flaps is believed to offer some restraint

to the build-up of the boundary layer in the region of the wing tip, the distance from the inboard end of the $0.45b/2$ leading-edge flap to the tip of the subject high-aspect-ratio wing is such as to allow a boundary-layer growth sufficient to precipitate flow separation. It would appear that more favorable stability characteristics could be obtained in the moderate lift range by combining the fences, which offer more of a restraint to the outflow of boundary-layer air, with leading-edge flaps which impart the benefits of camber to the outboard sections. Although no pressure-distribution measurements were made on the wing equipped with both leading-edge flaps and upper-surface fences, force data presented in reference 1 are available which indicate the favorable effects of upper-surface fences in linearizing the pitching-moment curve when used in conjunction with leading-edge flaps. Comparison of the pressure-distribution diagrams of the outboard sections of corresponding leading- and trailing-edge flap configuration with and without upper-surface fences (fig. 12) indicates that considerable gains in lift can be realized in the upper portion of the moderate lift range (which for the configuration with trailing-edge flaps deflected is from $C_L = 0.7$ to 1.2) when upper-surface fences are used in conjunction with leading-edge flaps. These gains in lift are more easily seen in figure 8 and the effects of these gains in lift on the over-all pitching moment are shown in figure 4 where a more nearly linear pitching-moment curve was obtained when fences were used in conjunction with leading-edge flaps than when leading-edge flaps were used alone.

High lift range ($C_L = 0.95$ through $C_{L_{max}}$).- Examination of the chordwise pressure diagrams of the basic wing (fig. 11) indicates that, from a lift coefficient of 0.95 ($\alpha = 18.0^\circ$) (see fig. 3) through maximum lift, flow separation which originated in the tip region continued to progress inboard so that at a lift coefficient of 1.0 ($\alpha = 20.0^\circ$) flow separation has spread inboard of the wing moment center ($\frac{2y}{b} = 0.43$); this effect resulted in an over-all pitching-moment curve which became progressively more unstable with lift coefficient up to a lift coefficient of 1.0. Beyond a lift coefficient of 1.0 ($\alpha = 26^\circ$ to 32°), the section lift curves indicate that the effectiveness of the tip sections increases along with a rearward movement of the chordwise centers of pressure for all sections (figs. 7 and 9). Thus, the combined effects of flow separation over the inboard part of the wing panel along with the increased lift effectiveness of the inboard sections and the accompanying rearward movement of the chordwise centers of pressure of both inboard and outboard sections resulted in a stable break in the over-all pitching-moment curve.

With upper fences installed, flow separation was delayed over the outboard portion of the wing until a lift coefficient of approximately 0.95 was attained (figs. 3 and 11). At an angle of attack of 20.6° (fig. 11(e)), which corresponds to a lift coefficient of approximately 1.0, flow

separation engulfed stations $\frac{2y}{b} = 0.55$ and 0.96 . As the angle of attack was increased further, flow separation spread over the entire outboard portion of the wing (fig. 11(f)). These results suggest that the localized regions of flow separation which occurred inboard of each upper-surface fence, and the effects of sweep on the induced-angle distribution along the wing span caused the sections of the outboard portion of the wing panel to attain values of maximum lift before those sections of the wing located inboard of the wing moment center. Consequently, an initial loss in lift occurred over the outboard wing sections and their negative pitching-moment contributions suddenly become more positive (fig. 5) resulting in a rather abrupt unstable break in the wing pitching-moment curve.

With leading-edge flaps deflected, the chordwise pressure-distribution diagrams indicate that, in the lift-coefficient range from 1.10 to 1.15 which corresponded to an angle-of-attack range from 19° to 22° (fig. 11(e)), considerable trailing-edge separation existed over the outboard panel of the wing. This separation is also reflected in the section lift curves by a decrease in lift-curve slope (fig. 7). In the lift-coefficient range beyond 1.15, stations $\frac{2y}{b} = 0.30$, 0.55 , and 0.96 show a marked decrease in lift. The extent of the inboard flow separation is more readily seen upon examination of the section lift curves where flow separation is indicated as far inboard as station $\frac{2y}{b} = 0.10$ between angles of attack of 25° and 29° . Although the leading-edge pressures of the flap generally decreased in the lift-coefficient range beyond 1.15 (fig. 11(f)), a complete breakdown in flow, as occurred on the basic wing with and without fences, did not occur over the outboard portion of the wing in the range of angles of attack investigated. The unstable trend in the pitching-moment curve in the lift-coefficient range from 1.10 to 1.15 would at first appear to result from the influence of trailing-edge separation on the outboard sections of the wing panel. The pitching-moment parameters, however, indicate that the unstable trend appears to result from tip effects at the outboard end of the leading-edge flap which induce flow separation (fig. 5). This result is substantiated by the section lift curves (fig. 7) which show a loss in lift effectiveness at station $\frac{2y}{b} = 0.96$ at an angle of attack of 19° which corresponds to the lift coefficient which marks the beginning of the unstable pitching-moment trend. In the lift-coefficient range beyond 1.15, the influence of flow separation inboard of the leading-edge flap has decreased the positive pitching-moment contributions of the inboard portion of the wing sufficiently to offset the effects of flow separation elsewhere on the wing panel so that a stable break in the over-all pitching-moment curve occurred.

Effect of Leading-Edge-Flap Span

The effect of a leading-edge flap of various spans on the pitching-moment characteristics of the subject wing are shown in figure 13. It can be seen that flaps produced unfavorable stability characteristics in the lower and upper portion of the moderate lift-coefficient range, respectively. The reasons, however, for the occurrence of the unfavorable stability characteristics are different in each case.

Flow considerations indicate that the vortex, which is generated at the inboard end of the leading-edge flap, offers some restraint to the outward drainage of the boundary-layer air and thereby dictates the length of the boundary-layer run over the outboard portion of the wing panel. In the case of a flap span greater than 45 percent of the semispan, therefore, the extent of the boundary-layer build-up and the subsequent flow separation over the outboard portion of the wing increased with flap span (fig. 14). Inasmuch as this flow separation, which is due to the accumulation of boundary-layer air over the trailing edge of the outboard portion of the wing, occurs for the wing with leading-edge flaps at moderate angles of attack, approximately 8° to 12° , it appears reasonable that the unfavorable stability characteristics which were obtained on the subject wing equipped with a $0.50b/2$ span leading-edge flap in the moderate angle-of-attack range resulted from increased trailing-edge flow separation over the outboard portion of the wing as compared to $0.40b/2$ leading-edge flaps. Based upon the knowledge of the inboard progression of flow separation with angle of attack, indications are that, as the leading-edge flap span is increased, the angle-of-attack range over which the stability characteristics would be influenced unfavorably would also increase. The shape of the pitching-moment curve for a full-span leading-edge flap configuration thus would be expected to approach that obtained for the basic wing (ref. 7).

For flap spans less than 45 percent of the wing semispan, the length of the boundary-layer run is decreased and therefore the extent of trailing-edge flow separation that occurs over the outboard sections at moderate angles of attack is also decreased (fig. 14). Consequently, an improvement in the stability of the subject wing would be expected in the lower portion of the angle-of-attack range in the vicinity of 8° . As the flap span is decreased to less than 45 percent of the semispan, however, flow separation which occurs at the inboard end of the leading-edge flap moved outboard of the wing moment center (fig. 15) so that poor stability characteristics were obtained in the angle-of-attack range at which this flow separation becomes predominant and which for the subject wing was approximately an angle of attack of 20° to 22° .

The optimum leading-edge flap span from stability considerations for the subject wing, therefore, is one which would allow the minimum degree

of trailing-edge separation to occur and yet position the flow separation that originates at the inboard end of the flap to occur inboard of the wing moment center.

Effect of Trailing-Edge Flaps

The most significant effect of variations in the span and type of trailing-edge flaps on the pitching-moment characteristics were changes in trim, since, within the range of trailing-edge flap spans investigated ($0.35b/2$ to $0.6b/2$, ref. 1), the pitching-moment characteristics were unsatisfactory in that the pitching-moment curves became unstable just below maximum lift. It is difficult therefore to evaluate the effect of varying span and type of trailing-edge flaps on the stability of the subject wing. It should be pointed out that these results should not be construed to be characteristic of other swept wings since the data of reference 8 indicate that the stability of a 47.7° sweptback wing of aspect ratio 5.1, which was equipped with a $0.45b/2$ span leading-edge flap, was affected adversely by increasing the trailing-edge flap span beyond 55 percent of the semispan. The pitching-moment curves for the wing equipped with leading-edge flaps and with and without trailing-edge flaps (figs. 3 and 4) indicate that the addition of either $0.5b/2$ span split or extended trailing-edge flap resulted in a positive trim change with the largest trim change occurring for the split flap configuration.

At a given wing lift coefficient the pitching-moment parameters $c_{m_c}'/4 \frac{q^2}{c^2}$ of the outboard sections were more negative with trailing-edge flaps neutral than with trailing-edge flaps deflected, whereas the pitching-moment parameters of the inboard sections were essentially the same or slightly more negative with flaps deflected (figs. 5 and 6). The addition of $0.5b/2$ trailing-edge flaps produced a large rearward movement in the chordwise centers of pressure for the inboard located sections with the largest rearward movement being obtained for the extended flap configuration (figs. 9 and 19). The addition of trailing-edge flaps had no significant effect on the location of the chordwise center of pressure of the outboard located sections. The greatest increment in section lift over the inboard portion of the wing panel was obtained with extended trailing-edge flaps (figs. 7 and 8). The rearward movement of the centers of pressure that was obtained for both trailing-edge flap configurations was apparently of sufficient magnitude to offset the increases in section lift so that the addition of $0.5b/2$ trailing-edge flaps had no or in the case of $0.5b/2$ extended trailing-edge flaps slightly reduced the pitching-moment parameters $c_{m_c}'/4 \frac{q^2}{c^2}$ of the inboard sections. As a result of the increase in section lift that occurred over the inboard part of the wing when trailing-edge flaps were deflected, the lift contributions of the

sections located outboard of the trailing-edge flaps would be less for a given wing lift coefficient when the trailing-edge flaps were deflected than when they were retracted (fig. 18). Since trailing-edge flaps did not influence the location of the chordwise centers of pressure, the pitching-moment parameters $c_{m_c} / \frac{c^2}{c_c^2}$ of the outboard located sections would be less negative at a given wing lift coefficient with flaps deflected than when they were retracted. Consequently, as a result of the balancing of the inboard and outboard section pitching-moment contributions, a positive trim change was obtained when trailing-edge flaps were deflected. The fact that extended trailing-edge flaps produced the greater increment in section lift over the inboard located sections resulted in further reductions in the section lift requirements of the outboard sections for a given wing lift coefficient (fig. 18). Although a positive trim change would be expected for the extended flap configuration which would exceed that which was obtained for the split flap configuration as a result of increased lift over the inboard sections, a rearward movement of the chordwise centers of pressure were also obtained with extended trailing-edge flaps which were sufficiently large to reduce the positive pitching-moment contributions of the inboard sections and thus offset the effect of the reductions in lift over the outboard located sections. Consequently, a less positive trim change was obtained for the extended flap configuration than for the split-flap configuration.

In light of the foregoing discussion it is reasonable to expect for the range of flap spans investigated that smaller positive trim changes would be obtained as the span of the trailing-edge flaps extended over a greater part of the wing span inasmuch as trailing-edge flaps produce a large rearward movement of the center of pressure over those sections affected by the flap. The pitching-moment contributions of the sections located inboard of the wing moment center therefore would remain essentially the same as those of the basic configuration whereas the pitching-moment contributions of sections located outboard of the wing moment center would become progressively more negative with increase in flap span.

Lift Characteristics

It is evident from an inspection of the lift characteristics presented in figure 3 that the addition of stall-control devices increased the lift-curve slope of the basic wing beyond a lift coefficient of about 0.35, as well as the maximum lift coefficient. Increments in maximum lift coefficient of 0.05 and 0.22 were obtained with upper-surface fences and leading-edge flaps, respectively. As brought out in the discussion of the longitudinal stability characteristics, the more favorable lift characteristics that were obtained when stall-control devices were

installed on the wing resulted primarily from improved flow conditions over the outboard located sections when upper-surface fences were employed and the induced camber imparted to the outboard sections when leading-edge flaps were deflected. It can be seen from figure 8 that in the moderate and high lift-coefficient range most of the lift on the outboard portion of the wing is carried by the forward portion of the wing chord including the leading-edge flaps as the result of the effective induced camber. From the chordwise distributions of those sections equipped with the leading-edge flap (figs. 11 and 12) it can be seen that essentially two negative pressure peaks are obtained on the sections spanned by the leading-edge flaps, one at the leading edge of the flap and the other at the juncture of the leading-edge flap and the wing. This same type of chordwise distribution was obtained in two-dimensional tests for a section having a droop nose flap (ref. 9). The author of reference 9 attributes the occurrence of two negative pressure peaks to laminar separation at the leading edge of the flap and subsequent reattachment. It appears reasonable, however, that two negative pressure peaks could also occur without separation from the variation in the rates of curvature on the upper surface of the airfoil with leading-edge flap deflected.

It is interesting to note from an inspection of the section lift curves (fig. 7) of the basic wing that, although the outward drainage of the boundary-layer air was detrimental to the outboard sections, it was probably beneficial to the inboard sections as indicated by the fact that lift coefficients were obtained on the inboard sections that exceeded values obtained in two-dimensional flow (fig. 16). Also of interest are the shapes of the chordwise pressure-distribution diagrams by which the various stations produced section lift coefficients which exceeded two-dimensional maximum lift values. The chordwise pressure distributions of station $\frac{2y}{b} = 0.30$ are similar to those which would be expected from trailing-edge suction in that high negative leading-edge pressures and unseparated flow near the trailing edge of the section were sustained beyond the two-dimensional maximum lift coefficient. The shape of the chordwise pressure-distribution diagrams of the root section is suggestive of sections having very large amounts of camber. In the case of stations $\frac{2y}{b} = 0.10$ and 0.30 for the highest angle of attack investigated, the shapes of the pressure diagrams are indicative of separated flow; however, the values of the upper-surface pressures varied from values of pressure coefficient of approximately -2.0 to -1.0 rather than the customary value of approximately -0.5 obtained for two-dimensional sections operating in separated flow. Similar chordwise pressure diagrams have been noted on wings having a leading-edge vortex. Probe studies, however, made during the course of this investigation failed to substantiate the existence of a leading-edge vortex on the subject wing; therefore, these rises in negative pressure may be associated with the three-dimensional effects on a swept wing.

Comparison of the data presented in figures 3 and 4 shows that trailing-edge high-lift devices produced increments in lift coefficient ranging from 0.4 to 0.5 in the linear lift-coefficient range and from 0.25 to 0.4 in the maximum lift coefficient, the extended trailing-edge flaps producing the greatest increments.

There has been some question from time to time regarding the source of effectiveness of extended trailing-edge flaps. Inspection of the chordwise loadings presented in figure 19 for both split and extended trailing-edge flaps at various angles of attack indicates that the effectiveness of the extended flap results from increasing the local chord of the section and not from increasing the values of the individual pressures of the chordwise loading. Comparison of the section lift curves obtained for the split and extended trailing-edge-flap configurations (fig. 8) indicates that the lift increment that was obtained with extended flaps results, for the most part, from the increase in lift contributed by the inboard sections and, furthermore, that these increments decreased as the end of the flap is approached so that the increment of lift contributed by the outboard end of the extended flap is nearly equal to that contributed by the split flap.

CONCLUDING REMARKS

From a pressure-distribution investigation of the low-speed lift and pitching-moment characteristics of a 45° sweptback wing of aspect ratio 8 with and without high-lift and stall-control devices at a Reynolds number of 4.0×10^6 , the following remarks can be made:

Although it was not positively established, the results indicate that the instability of the basic wing, which began to occur at a lift coefficient of approximately 0.25, was due to flow separation over the outer 4 percent of the semispan of the wing. This flow separation was not reflected in the lift characteristics but, owing to the large moment arm involved, had significant effects on the pitching-moment characteristics. In the lift-coefficient range beyond a lift coefficient of 0.3 instability resulted from the inboard spread of flow separation over the outboard panel of the wing.

The use of either upper-surface fences or leading-edge flaps improved the stability and lift characteristics of the basic wing in the upper portion of the lift-coefficient range through the ability of these devices to improve the flow characteristics over the outboard panel of the wing.

For a given lift coefficient the positive trim change that occurred when trailing-edge flaps were deflected resulted from a combination of

[REDACTED]

a decrease in loading over the tip sections and a rearward shift in the chordwise centers of pressure over the inboard sections of the wing.

The rearward movement of the centers of pressures over the inboard sections that was obtained when trailing-edge flaps were deflected was greater for the extended flaps than for split flaps; this movement resulted in a trim change that was less positive for the extended flaps than for split flaps.

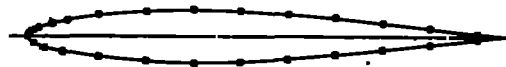
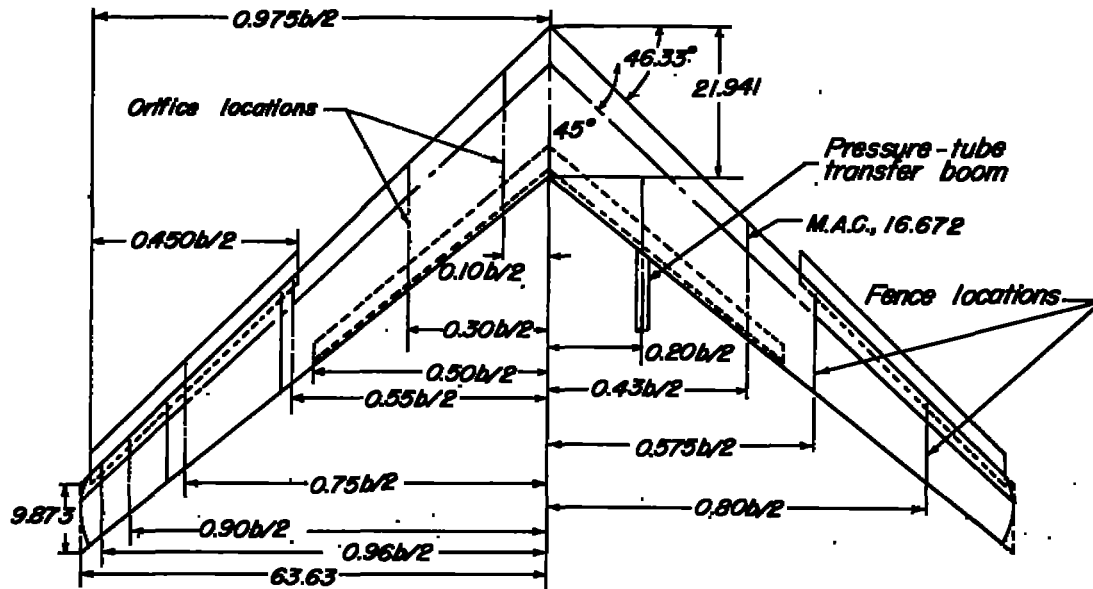
The increased lift effectiveness of the extended trailing-edge flaps was due to the increased chord of the sections spanned by the flaps rather than by increasing the individual pressures acting on sections.

Langley Aeronautical Laboratory,
National Advisory Committee for Aeronautics,
Langley Field, Va.

[REDACTED]

REFERENCES

1. Pratt, George L., and Shields, E. Rousseau: Low-Speed Longitudinal Characteristics of a 45° Sweptback Wing of Aspect Ratio 8 With High-Lift and Stall-Control Devices at Reynolds Numbers From 1,500,000 to 4,800,000. NACA RM L51J04, 1952.
2. Graham, Robert R.: Low-Speed Characteristics of a 45° Sweptback Wing of Aspect Ratio 8 From Pressure Distributions and Force Tests at Reynolds Numbers From 1,500,000 to 4,800,000. NACA RM L51H13, 1951.
3. Sivells, James C., and Salmi, Rachel M.: Jet-Boundary Corrections for Complete and Semispan Swept Wings in Closed Circular Wind Tunnels. NACA TN 2454, 1951.
4. Maki, Ralph L.: The Use of Two-Dimensional Section Data To Estimate the Low-Speed Wing Lift Coefficient at Which Section Stall First Appears on a Swept Wing. NACA RM A51E15, 1951.
5. Abbott, Ira H., Von Doenhoff, Albert E., and Stivers, Louis S., Jr.: Summary of Airfoil Data. NACA Rep. 824, 1945. (Supersedes NACA ACR L5C05.)
6. Jones, Robert T.: Effects of Sweepback on Boundary Layer and Separation. NACA Rep. 884, 1947. (Supersedes NACA TN 1402.)
7. Guryansky, Eugene R., and Lipson, Stanley: Effect of High-Lift Devices on the Longitudinal and Lateral Characteristics of a 45° Sweptback Wing With Symmetrical Circular-Arc Sections. NACA RM L8D06, 1948.
8. Salmi, Reino J.: Effects of Leading-Edge Devices and Trailing-Edge Flaps on Longitudinal Characteristics of Two 47.7° Sweptback Wings of Aspect Ratios 5.1 and 6.0 at a Reynolds Number of 6.0×10^6 . NACA RM L50F20, 1950.
9. Kelly, John A.: Effects of Modifications to the Leading-Edge Region on the Stalling Characteristics of the NACA 63₁-012 Airfoil Section. NACA TN 2228, 1950.



Typical plain wing section
parallel to plane of symmetry
NACA 63, A012

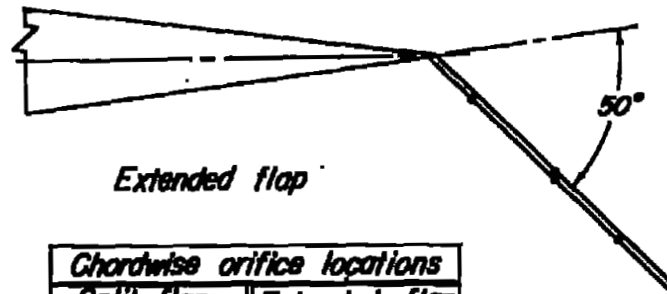
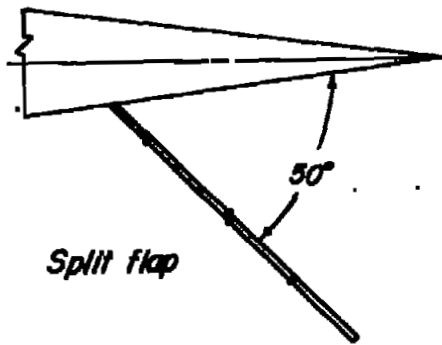


Chordwise orifice locations

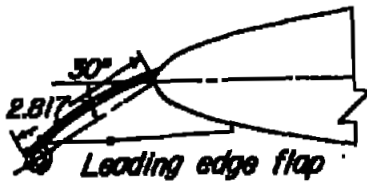
Upper surface				Lower surface			
X/C	Z/C	X/C	Z/C	X/C	Z/C	X/C	Z/C
0	0	.25	.0566	.0125	-.0149	.45	-.0597
.001	.0045	.35	.0600			.55	-.0515
.0025	.0069	.45	.0579	.0375	-.0254	.65	-.0419
.0050	.0093	.55	.0515			.75	-.0303
.0125	.0149	.65	.0419	.075	-.0350	.85	-.0183
.0250	.0208	.75	.0303			.95	-.0063
.050	.0290	.85	.0183	.15	-.0475		
.085	.0371	.95	.0063	.25	-.0566		
.15	.0475			.35	-.0600		

(a) Plain-wing chordwise and spanwise orifice locations.

Figure 1.- Layout of 45° sweptback wing equipped with high-lift and stall-control devices. All dimensions are in inches unless otherwise noted.

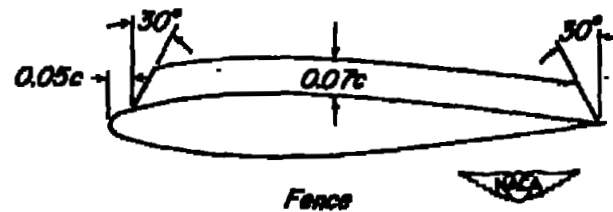


Chordwise orifice locations			
Split flap		Extended flap	
X/C	Z/C	X/C	Z/C
0.824	-0.047	1.024	-0.022
.870	-.088	1.070	-.064
.873	-.092	1.073	-.068
.910	-.125	1.110	-.101



Chordwise orifice locations	
*X/C	*Z/C
-0.040	-0.006
-.084	-.027
-.118	-.047
-.140	-.062
-.156	-.076
-.155	-.086
-.139	-.093
-.053	-.060

* Sta. $2y/b = 0.55$



(b) Details of high-lift and stall-control devices. All sections taken parallel to the plane of symmetry. All dimensions are in inches unless otherwise noted.

Figure 1.- Concluded.

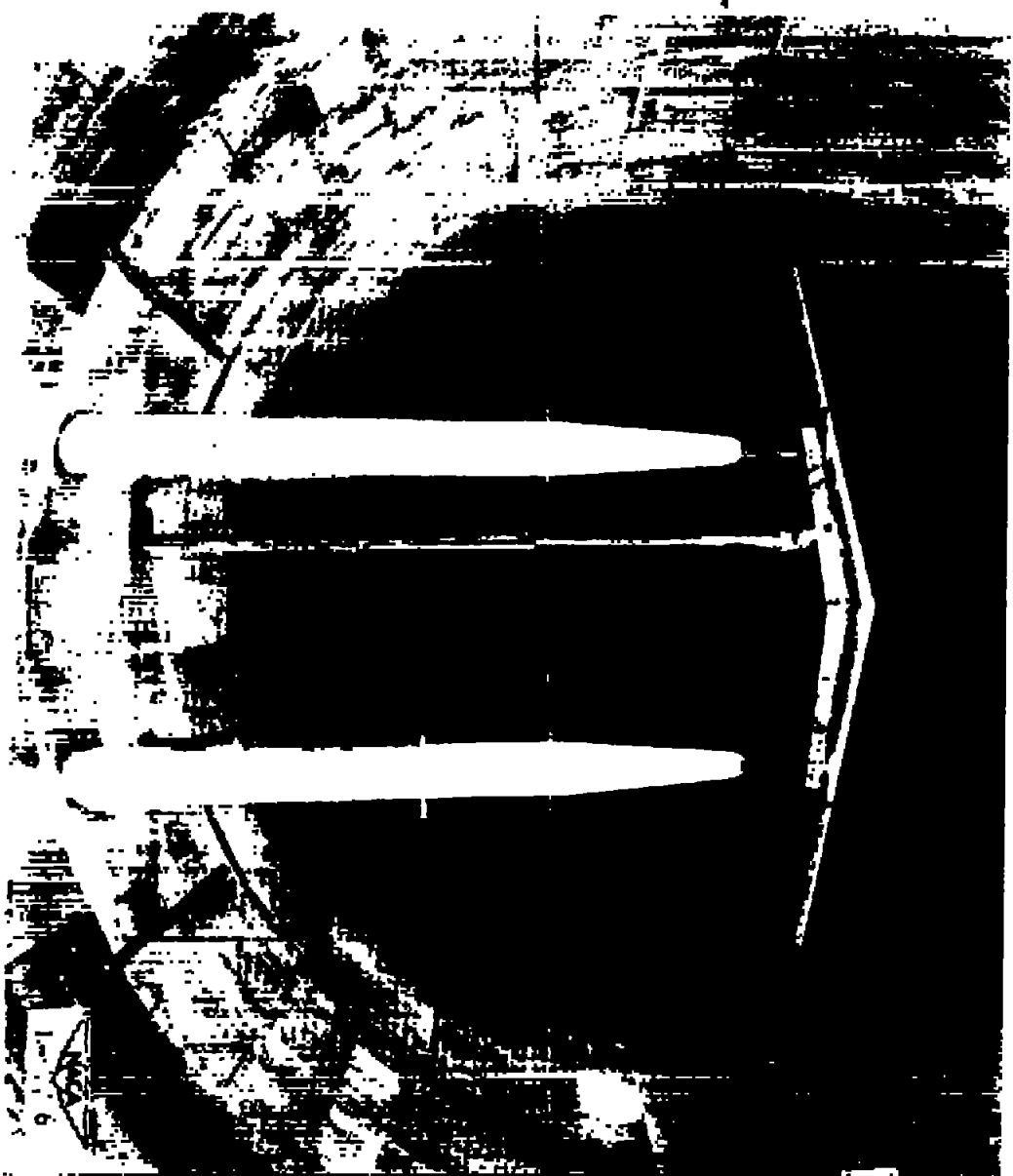


Figure 2.-- 45° sweptback wing mounted in the 19-foot pressure tunnel with pressure-tube system installed.

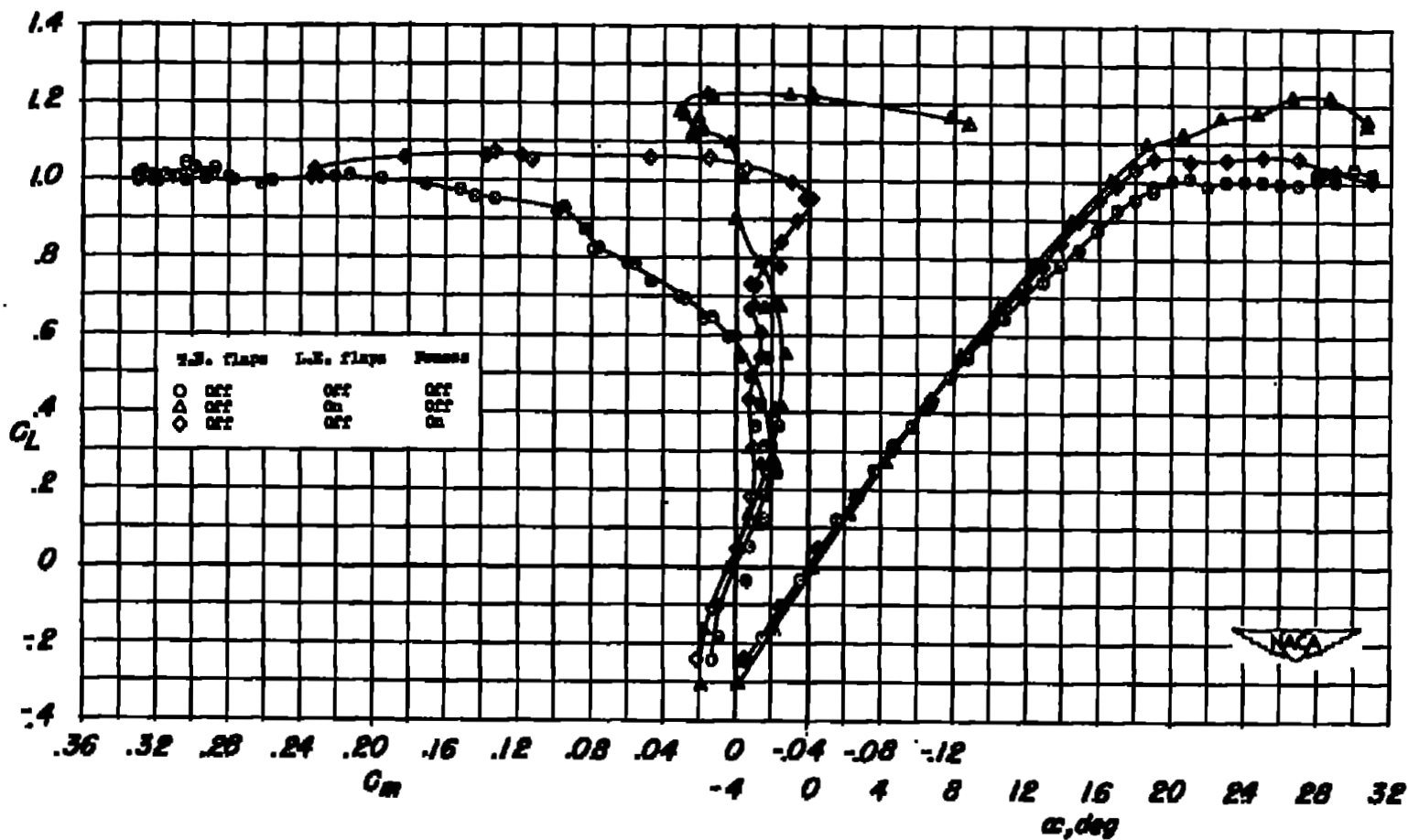


Figure 3.- Lift and pitching-moment characteristics of the wing with and without stall-control devices installed.

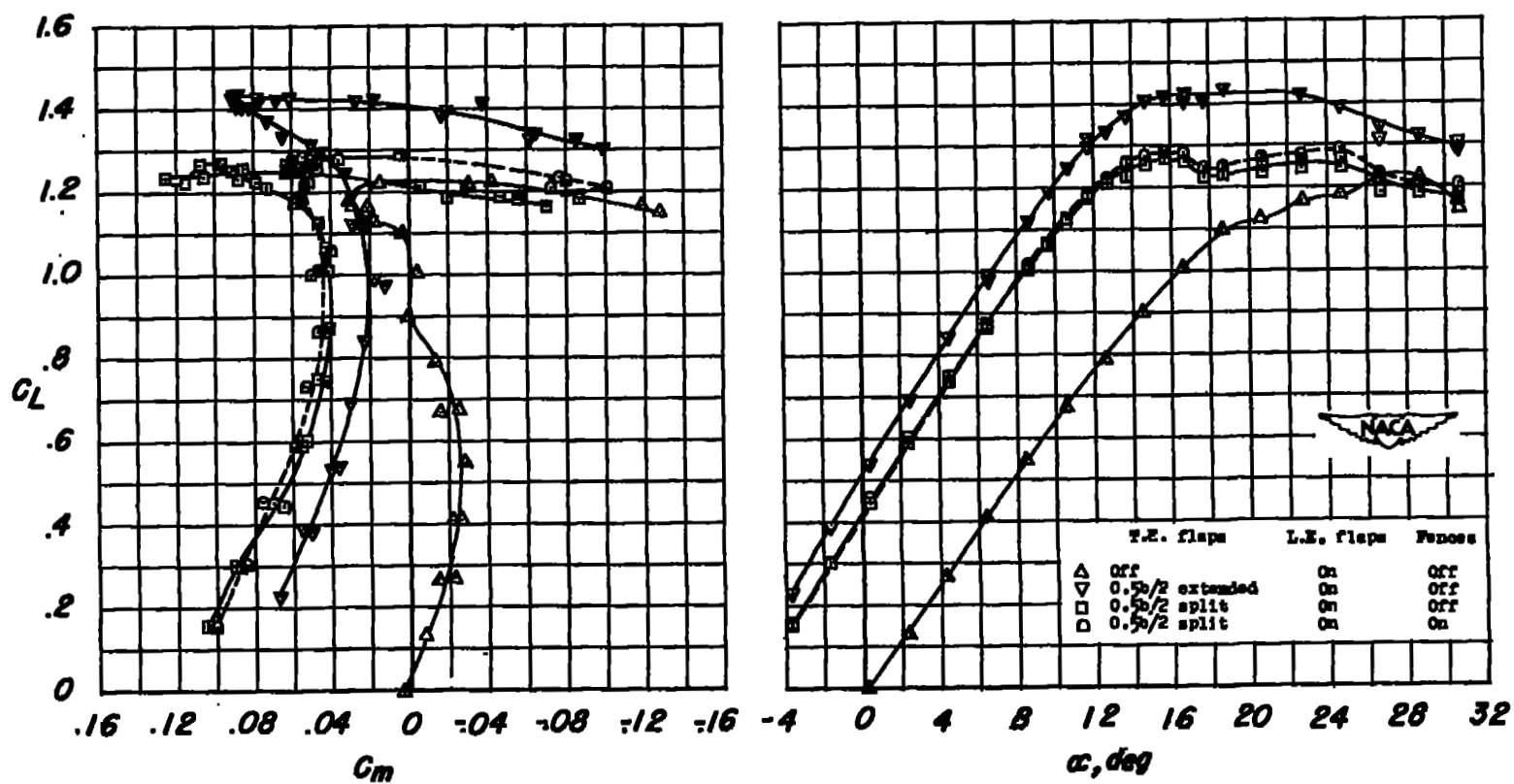
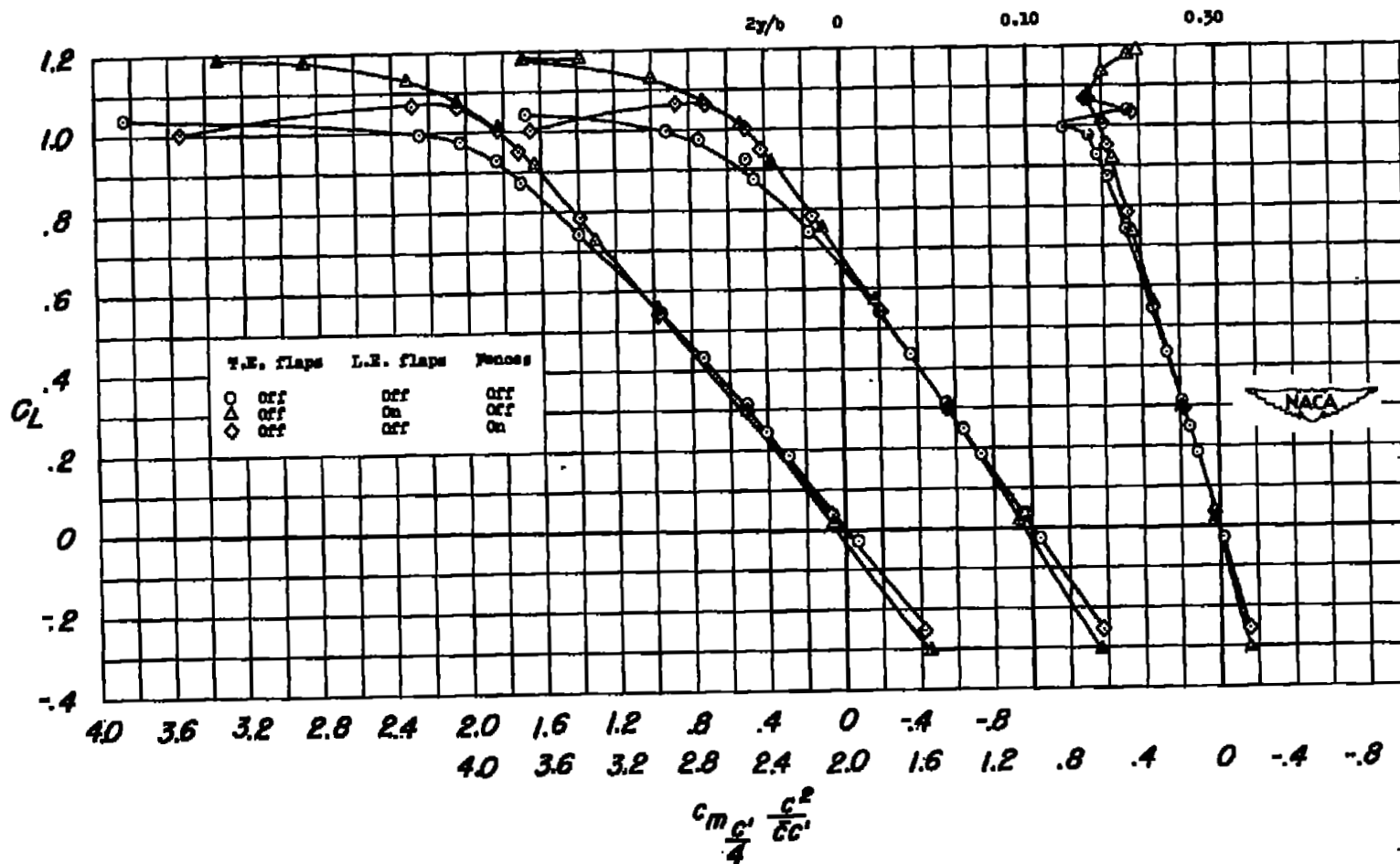
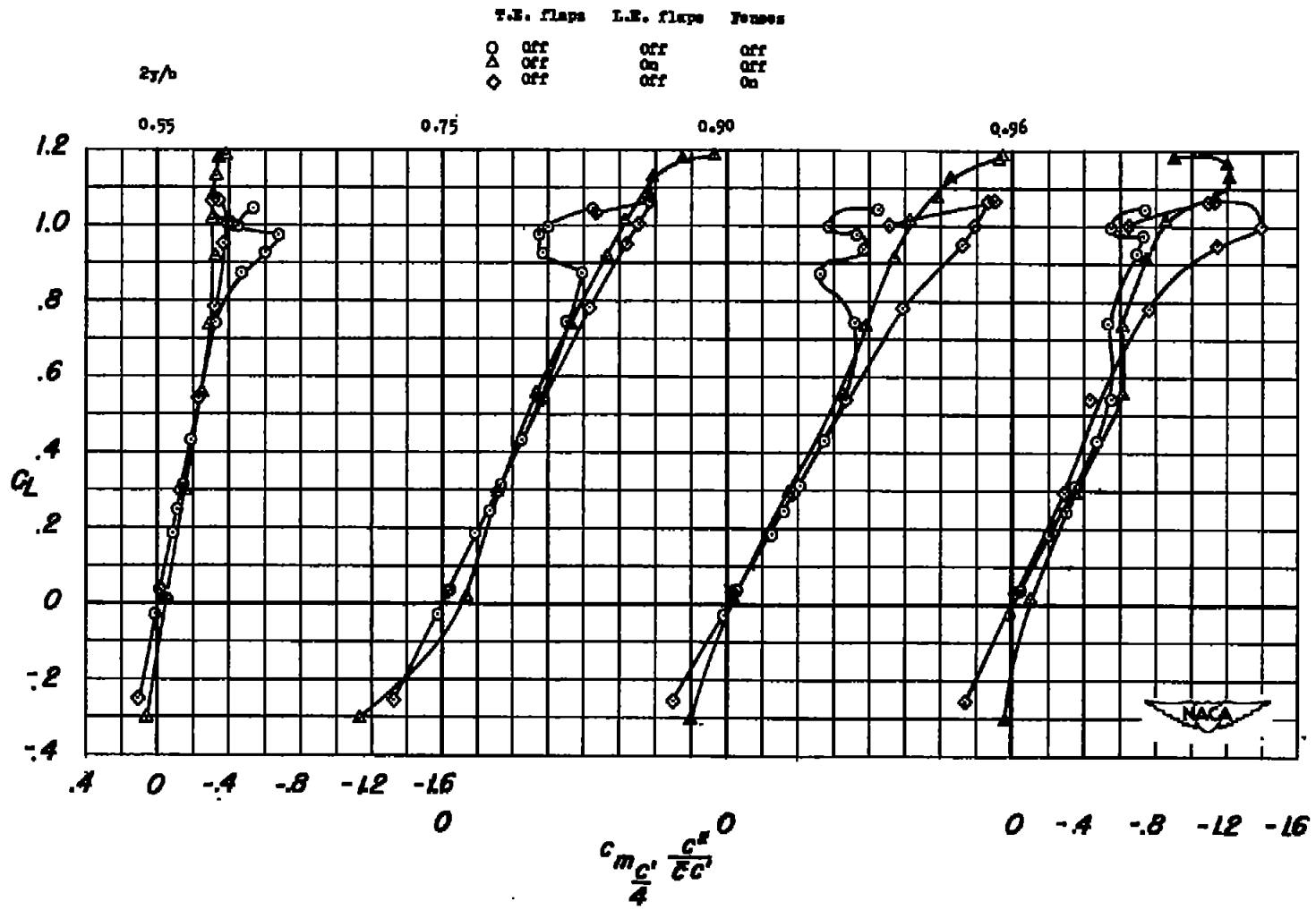


Figure 4.-- Lift and pitching-moment characteristics of the wing with high-lift devices and stall-control devices installed.



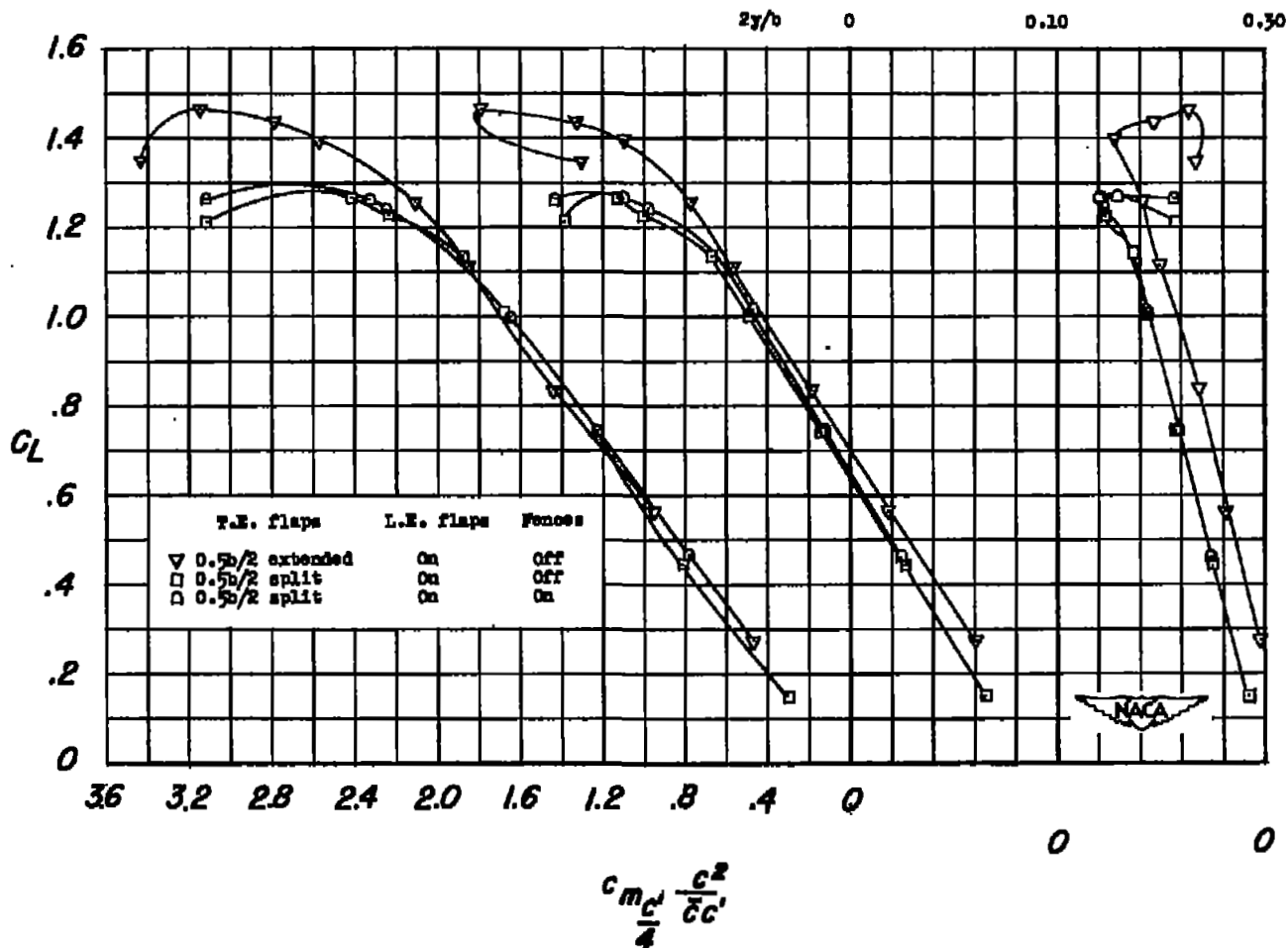
(a) Sections located inboard of $c'/4$.

Figure 5.- Section weighted pitching-moment characteristics of the wing with and without stall-control devices installed.



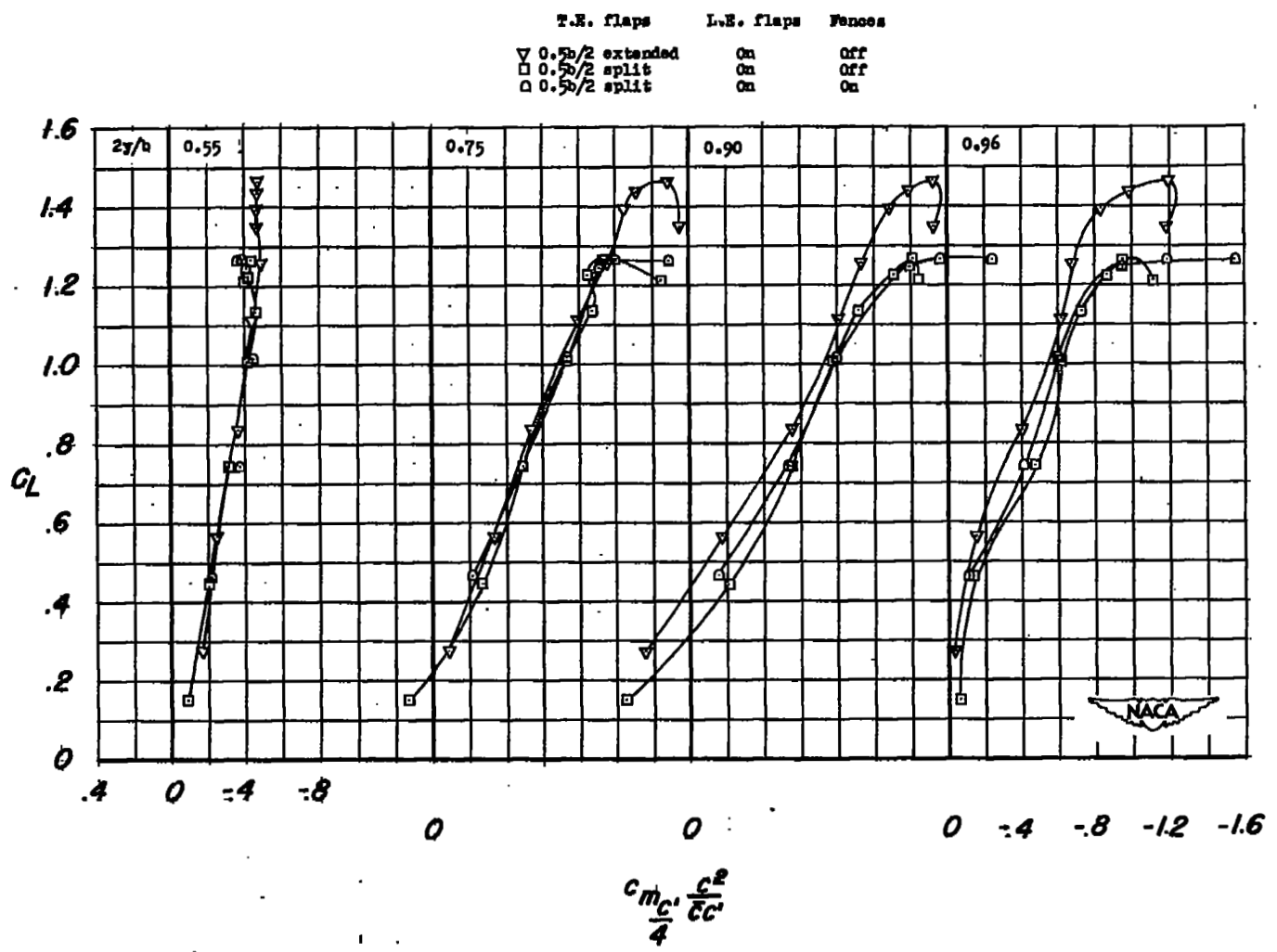
(b) Sections located outboard of $c'/4$.

Figure 5.- Concluded.



(a) Sections located inboard of $c'/4$.

Figure 6.- Section weighted pitching-moment characteristics of the wing with high-lift and stall-control devices installed.



(b) Sections located outboard of $c'/4$.

Figure 6.- Concluded.

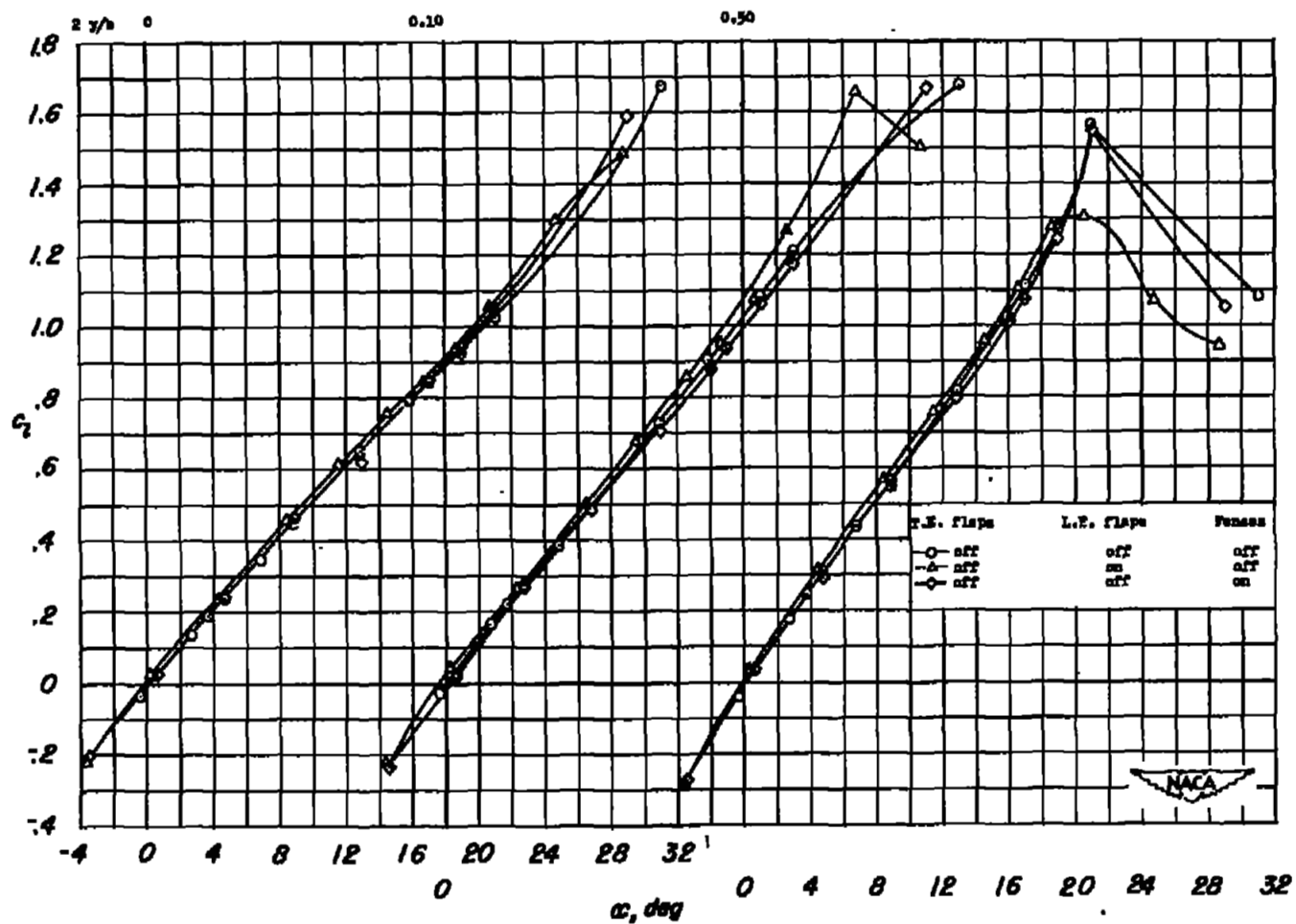
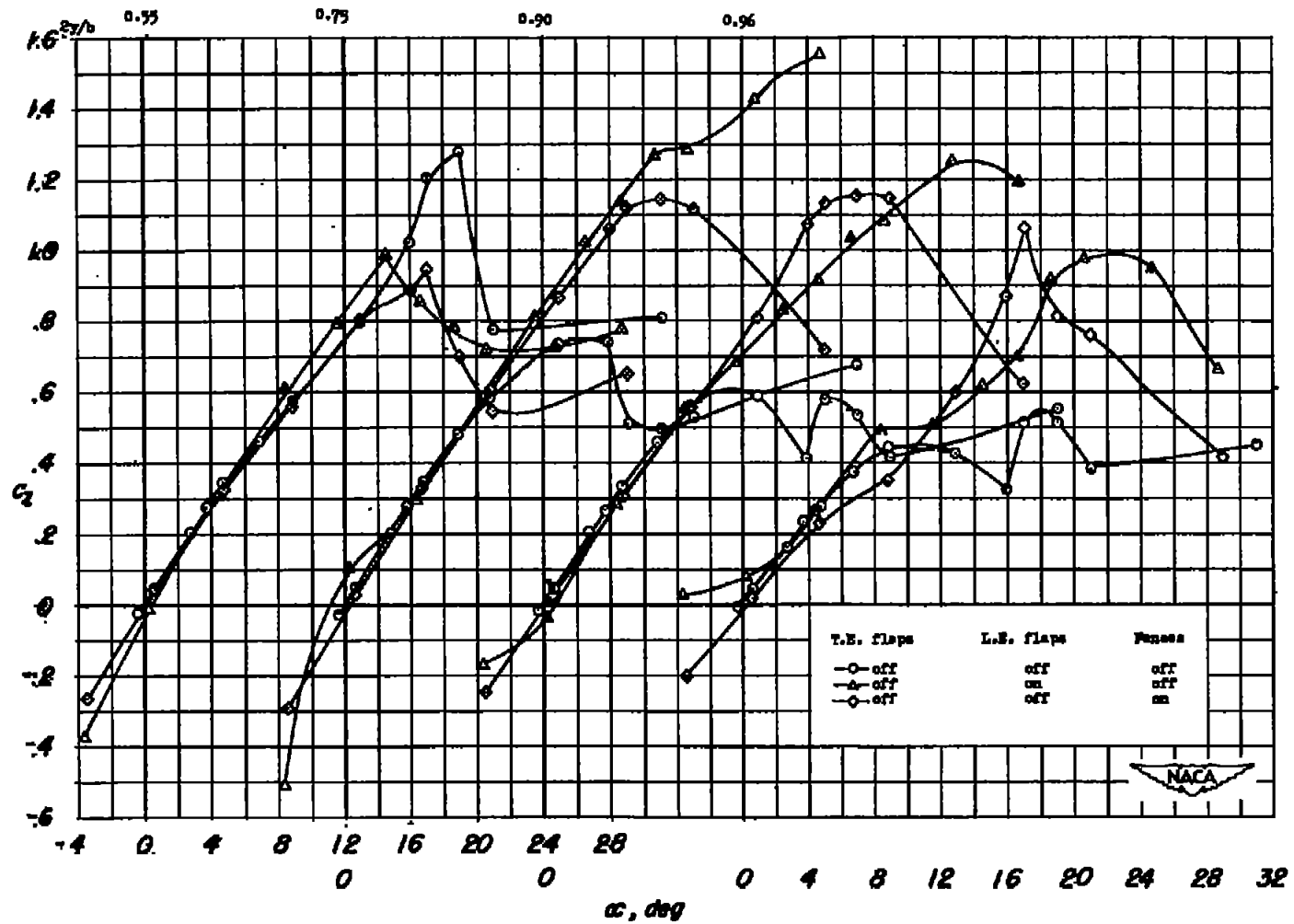
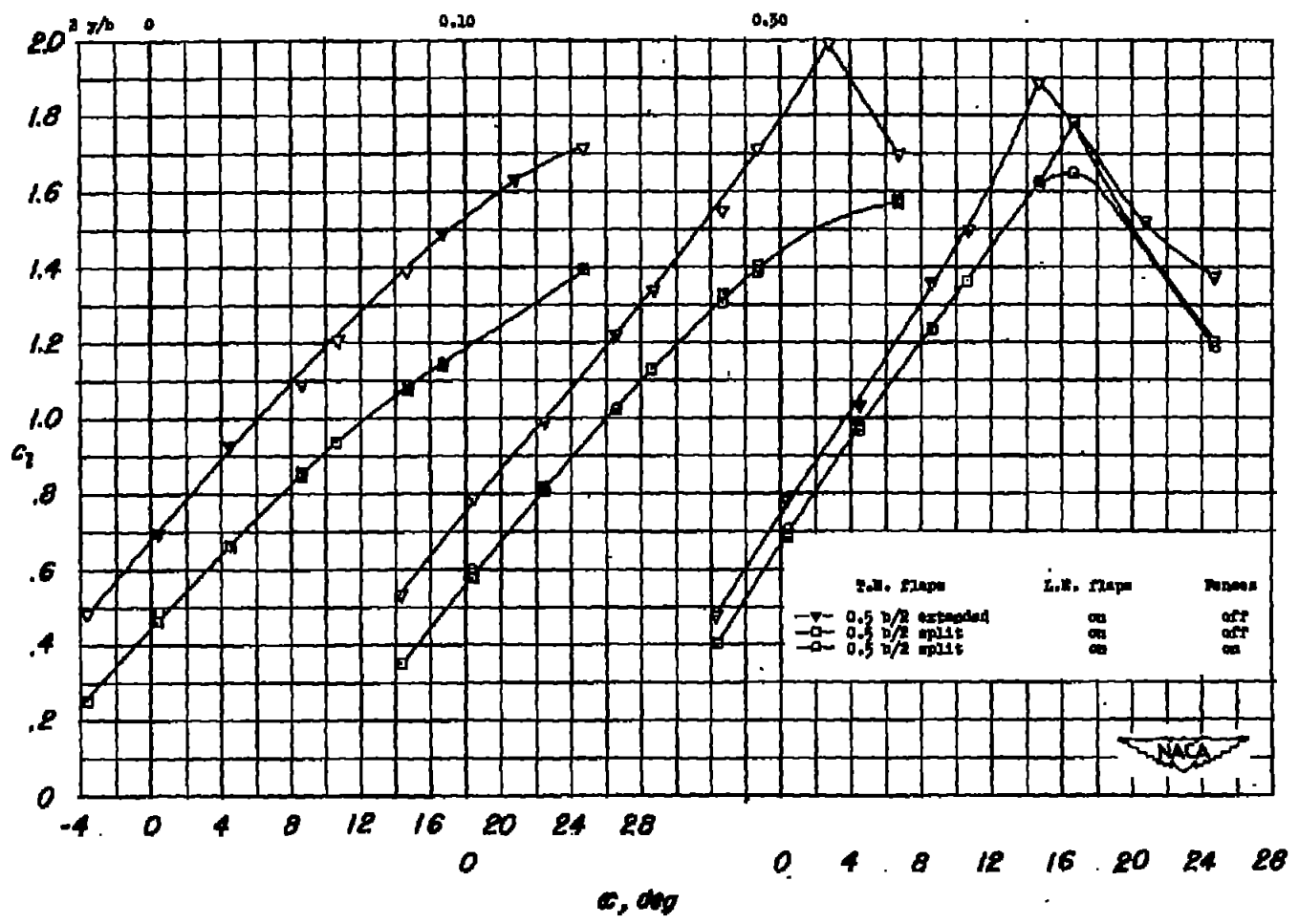
(a) Sections located inboard of $c'/4$.

Figure 7.- Variations of section lift coefficients with angle of attack for the wing with and without stall-control devices installed.



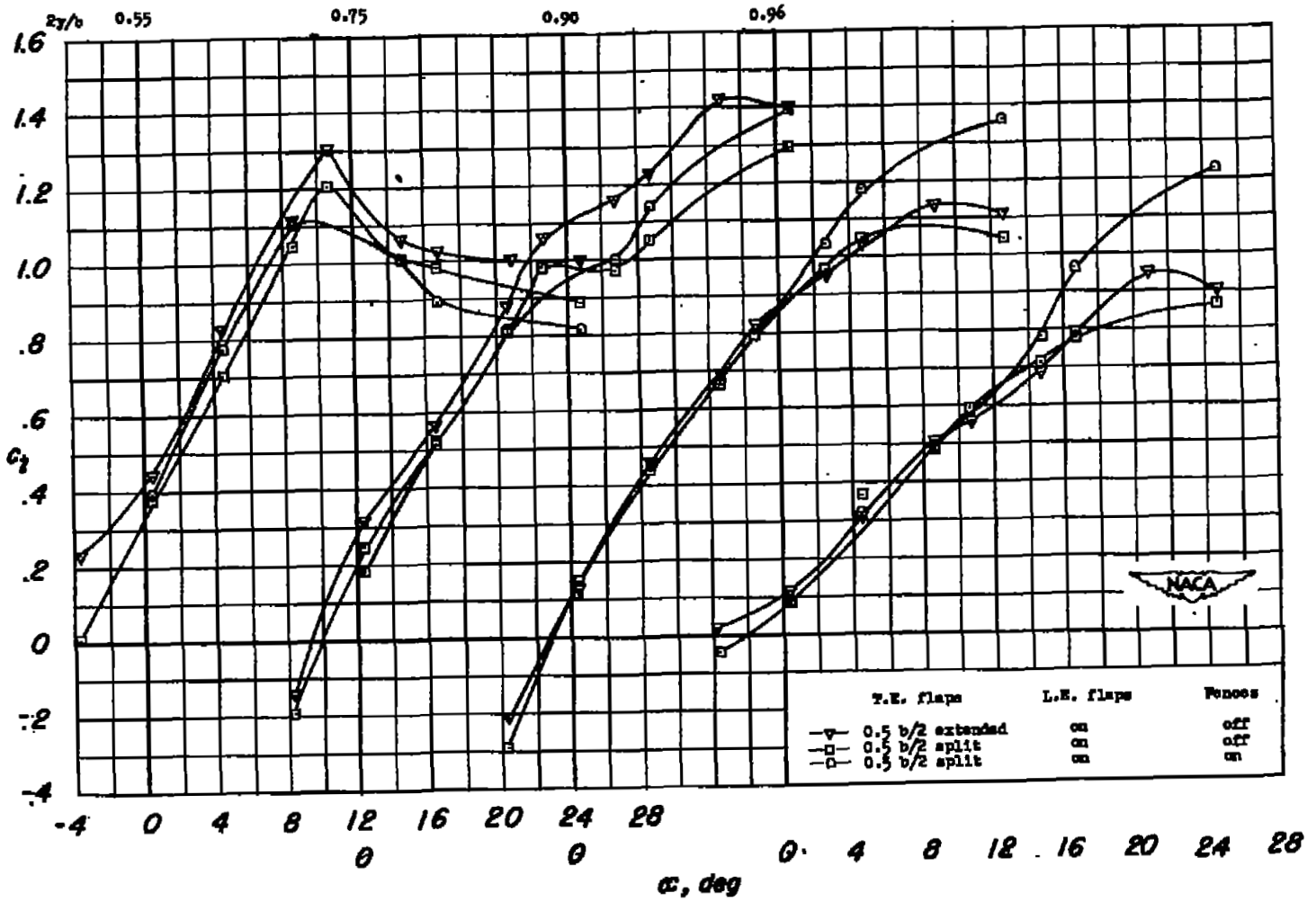
(b) Sections located outboard of $c'/4$.

Figure 7.- Concluded.



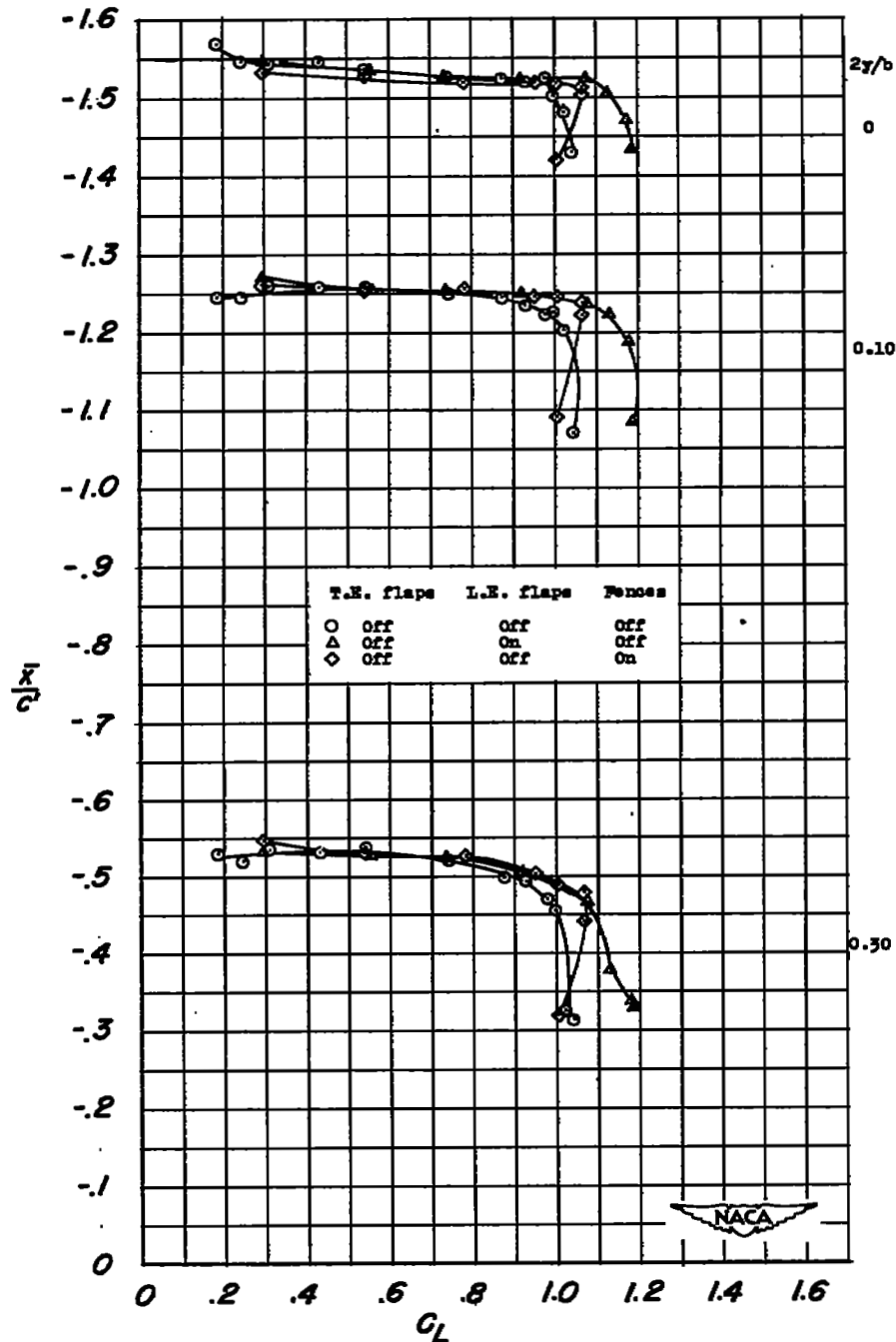
(a) Sections located inboard of $c'/4$.

Figure 8.- Variations of section lift coefficients with angle of attack for the wing with high-lift and stall-control devices installed.



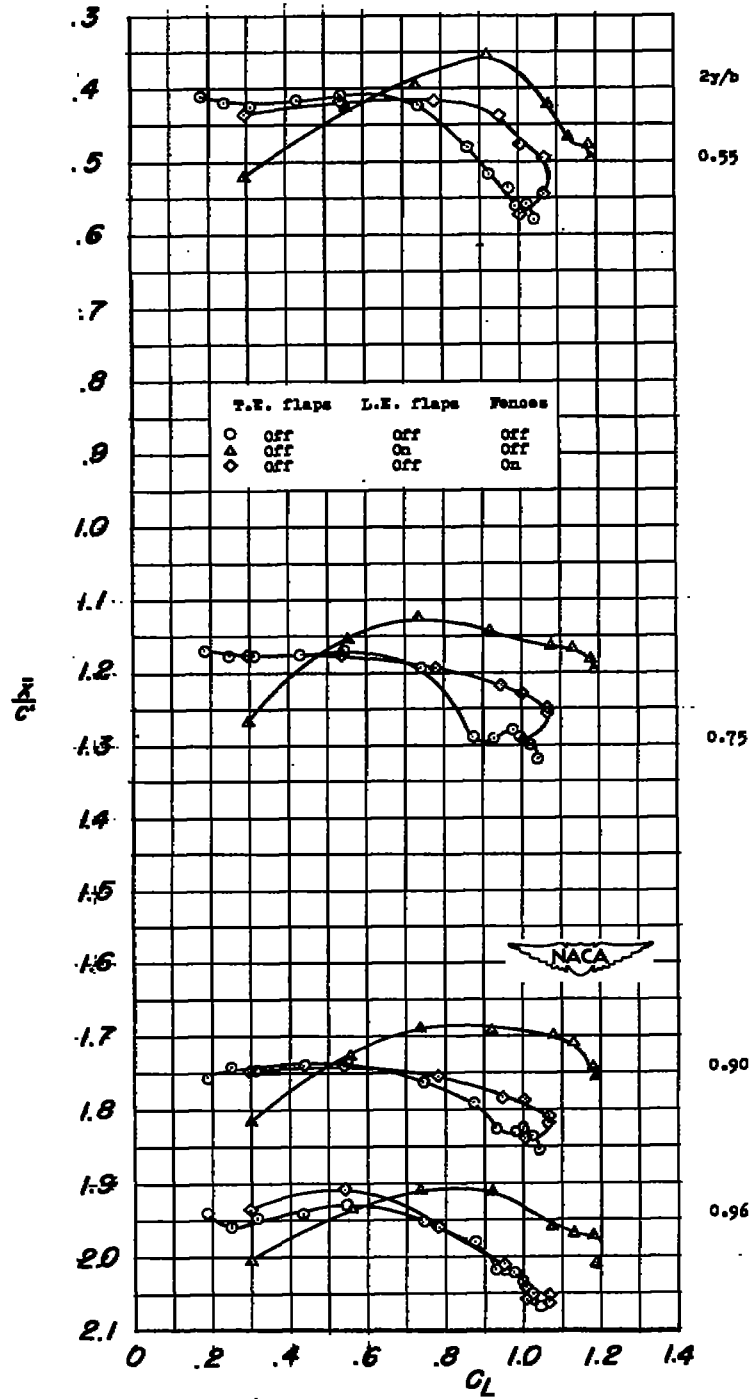
(b) Sections located outboard of $c'/4$.

Figure 8.- Concluded.



(a) Sections located inboard of $c'/4$.

Figure 9.- Variations of section center of pressure with lift coefficient for the wing with and without stall-control devices installed.



(b) Sections located outboard of $c'/4$.

Figure 9.- Concluded.

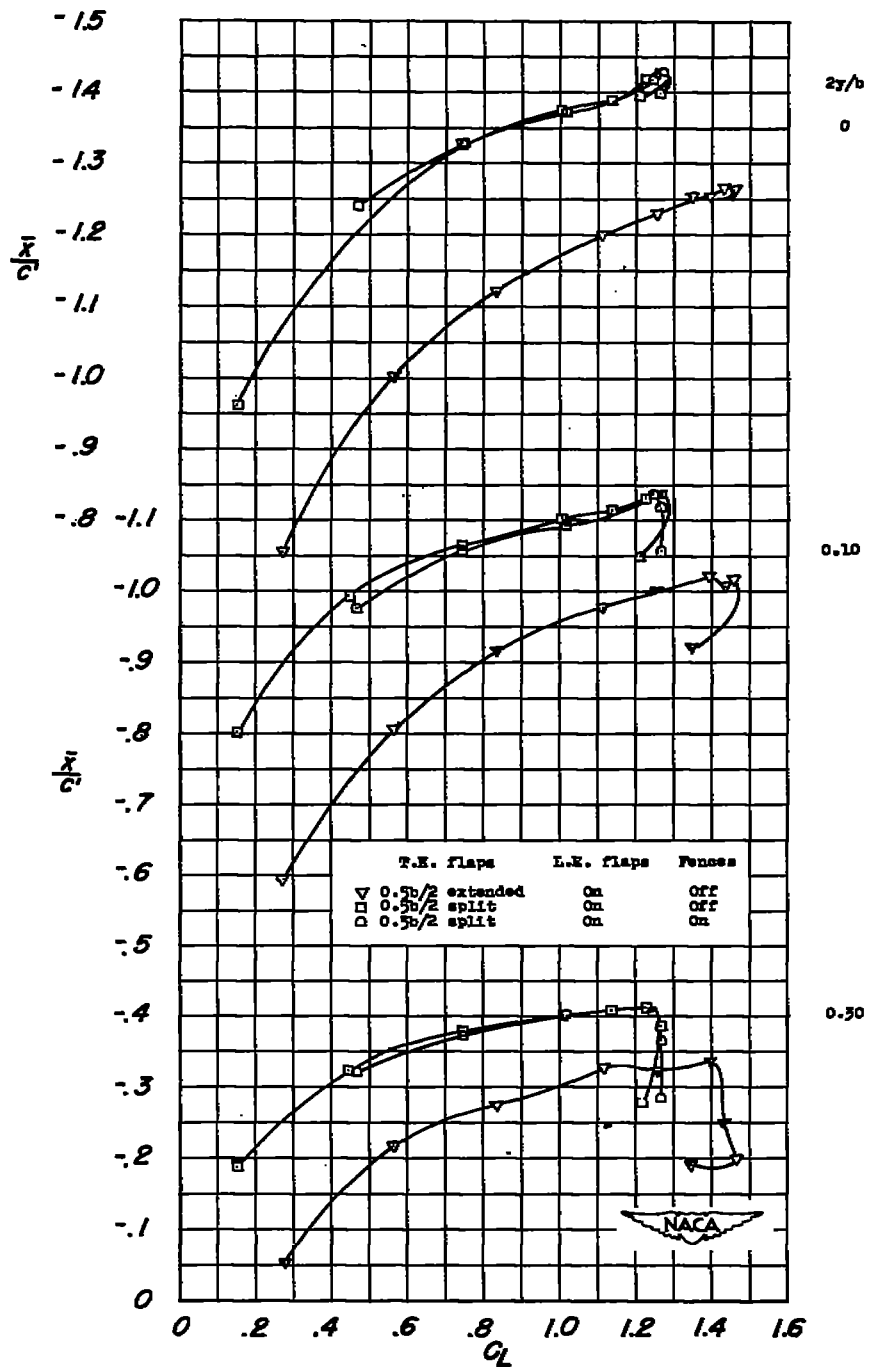
(a) Sections located inboard of $c'/4$.

Figure 10.- Variation of centers of pressures with lift coefficient for the wing with high-lift and stall-control devices installed.

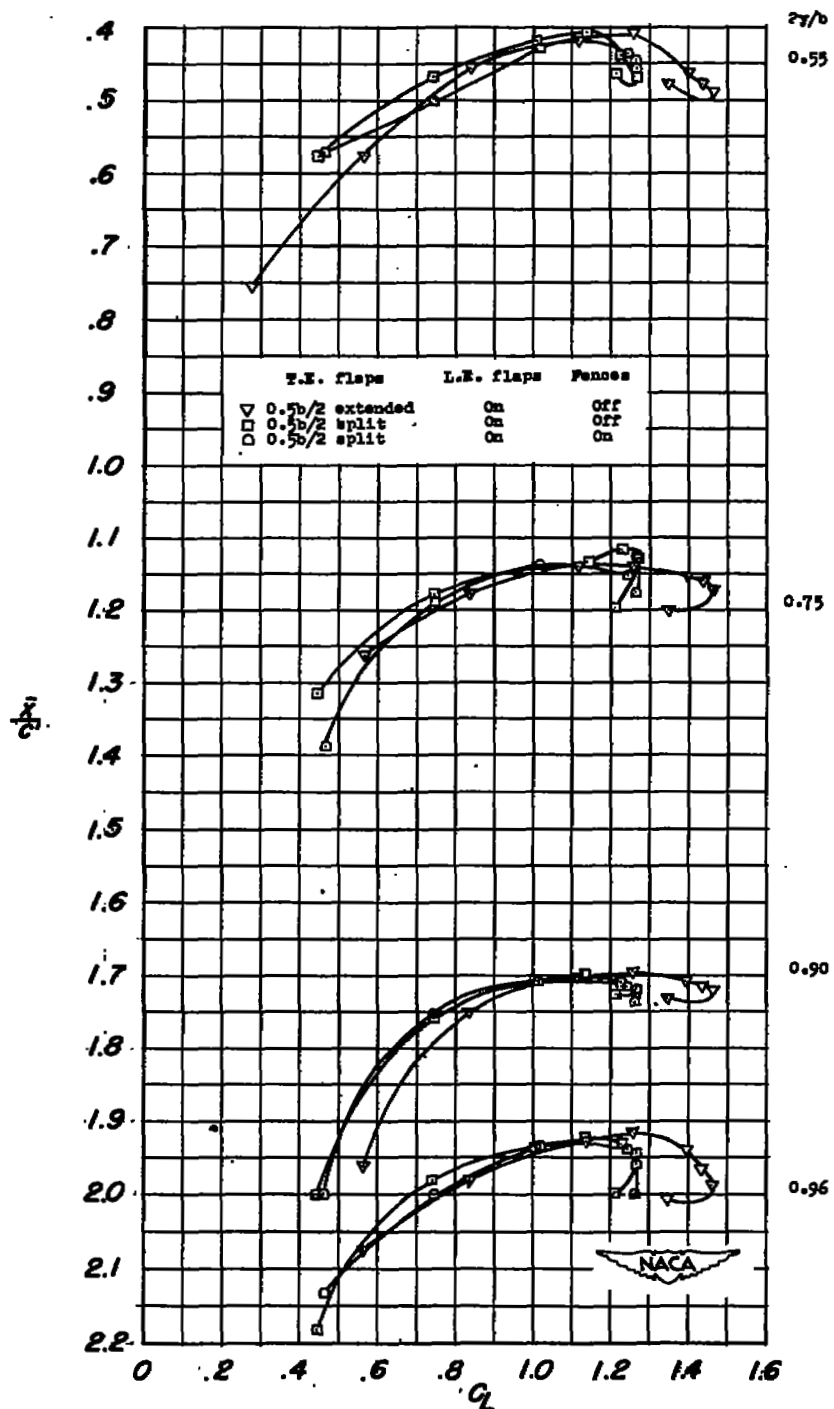
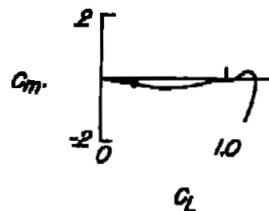
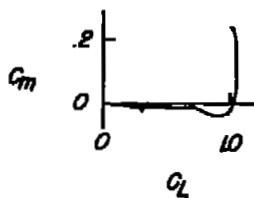
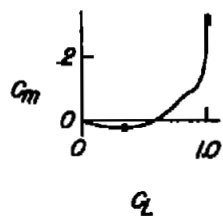
(b) Sections located outboard of $c' / 4$.

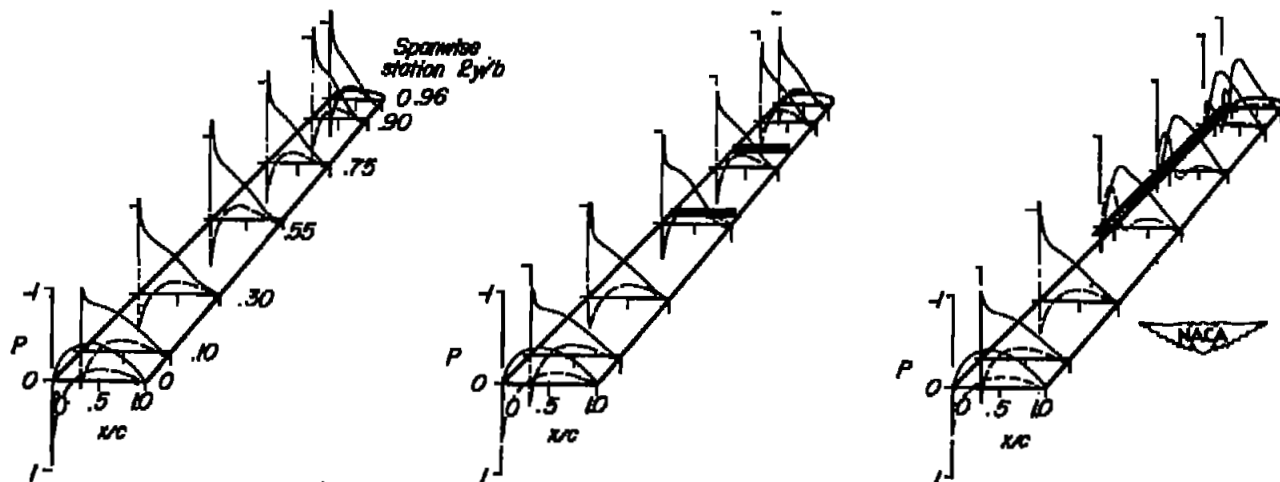
Figure 10.- Concluded.



Plain wing

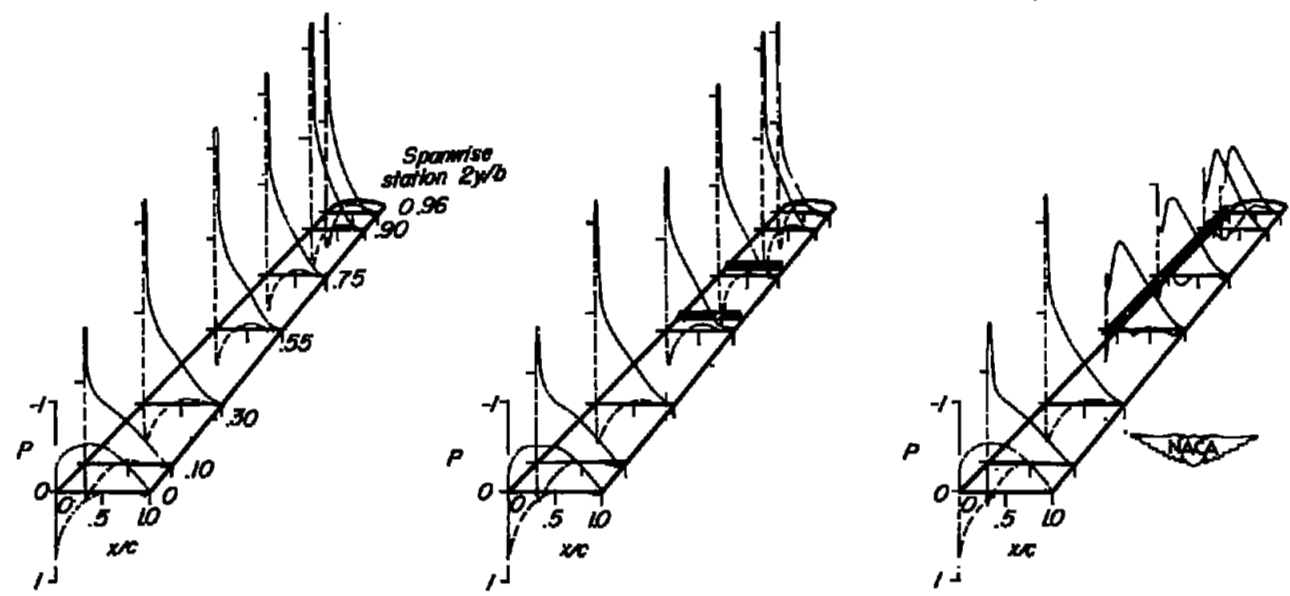
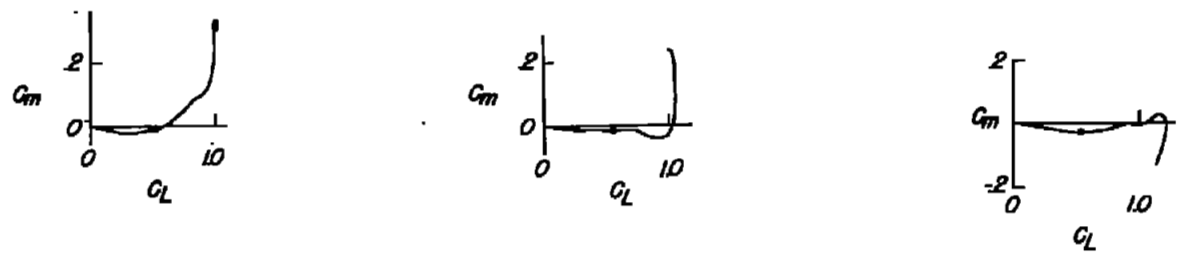
Upper-surface fences at
0.575b/2 and 0.80b/2

0.45b/2 leading-edge flaps



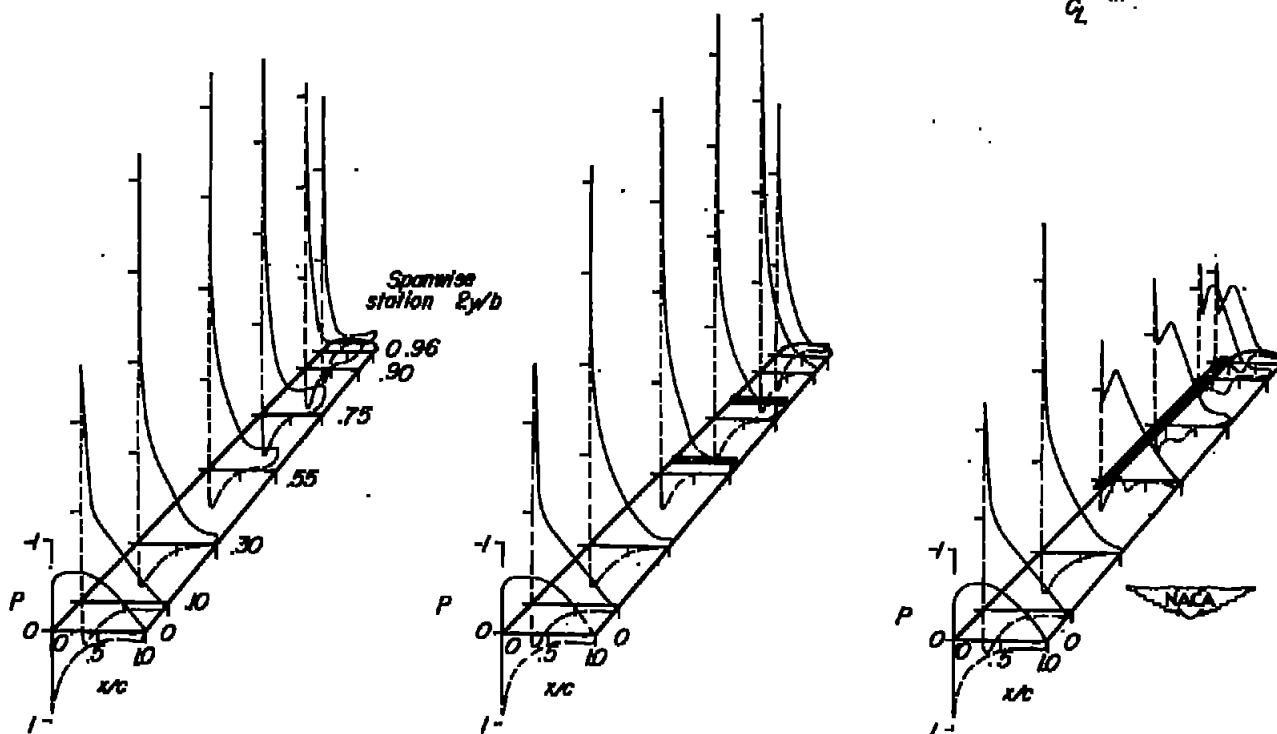
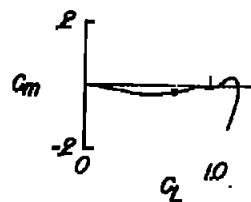
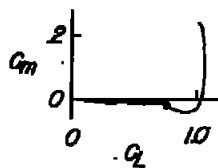
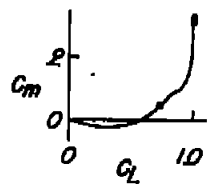
(a) $\alpha \approx 4.5^\circ$.

Figure 11.- Chordwise pressure distribution of the wing with and without stall-control devices installed.



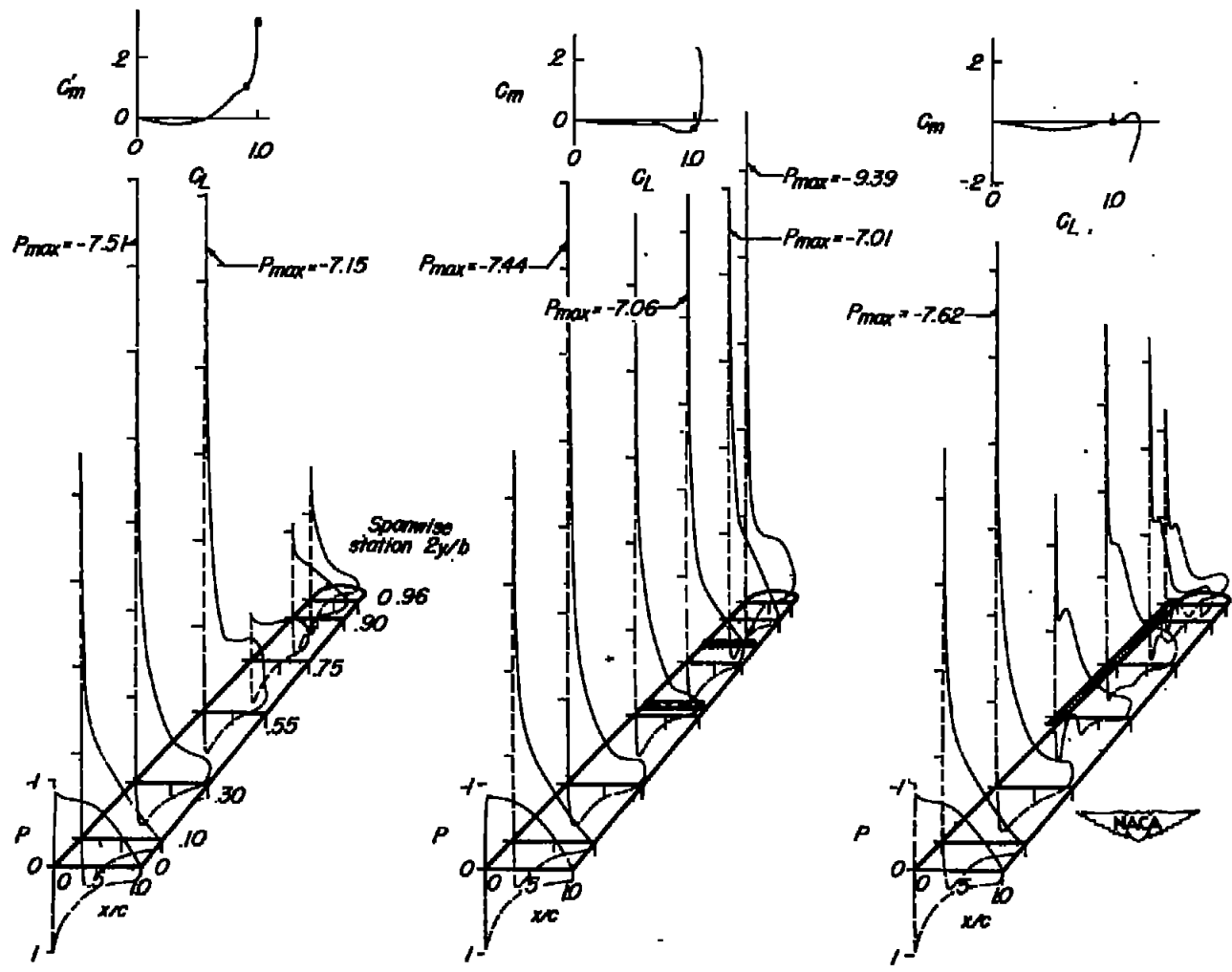
(b) $\alpha \approx 8.6^\circ$.

Figure 11.- Continued.



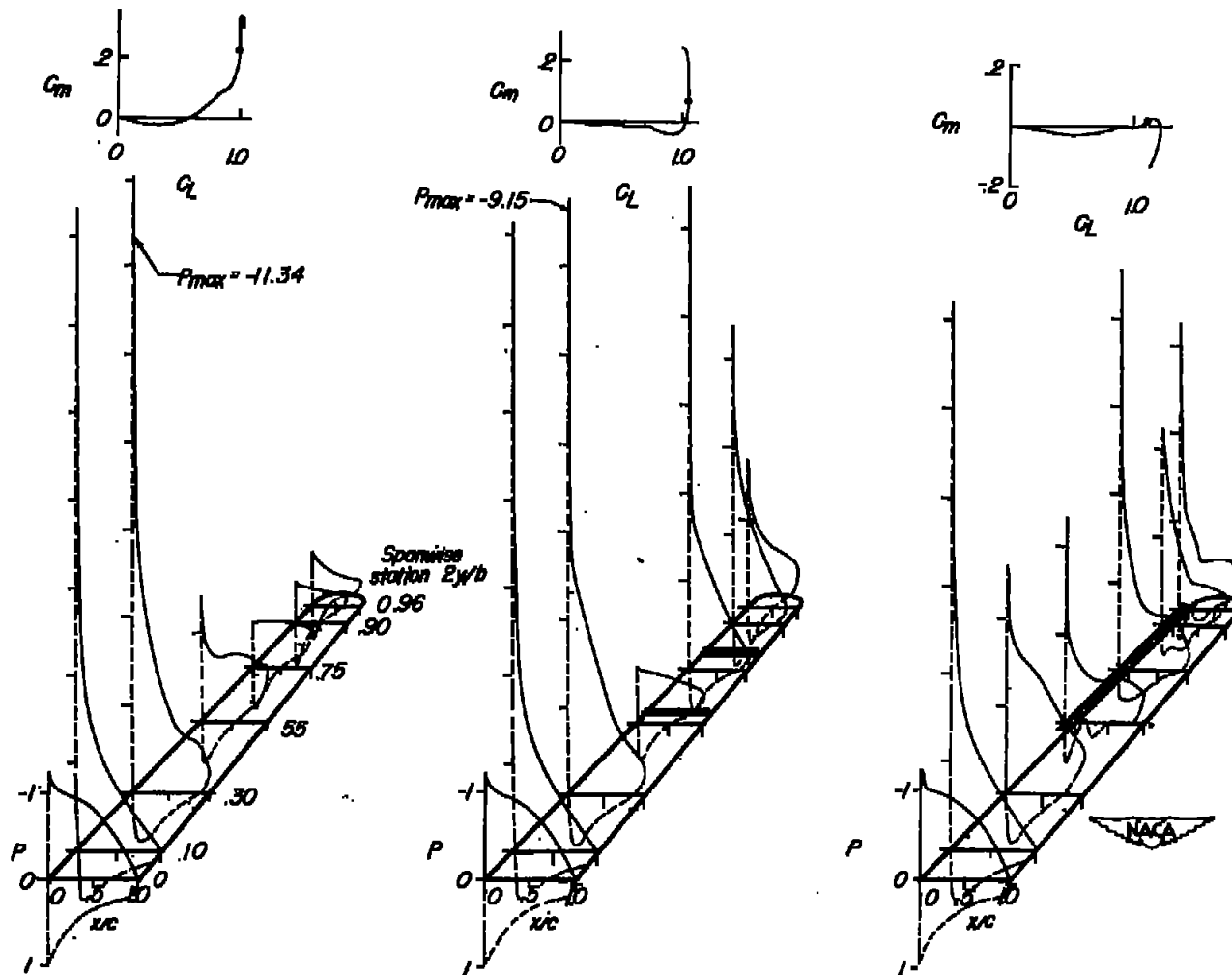
(c) $\alpha \approx 12.7^\circ$.

Figure 11.- Continued.



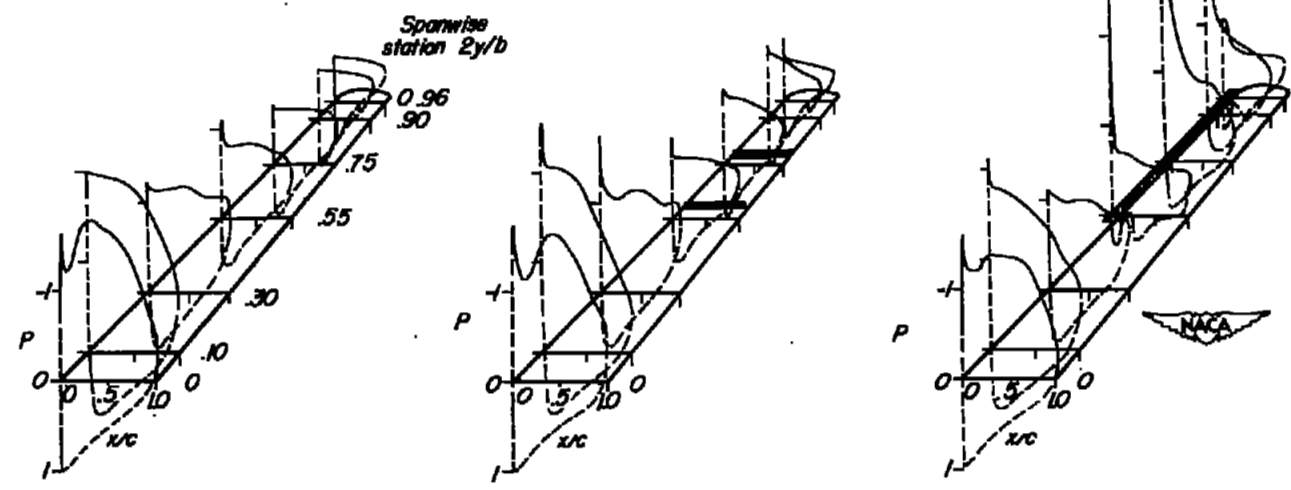
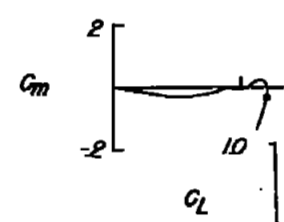
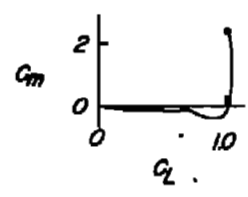
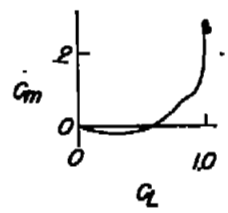
(d) $\alpha \approx 16.8^\circ$.

Figure 11.- Continued.



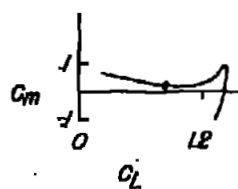
(e) $\alpha \approx 20.8^\circ$.

Figure 11.- Continued.

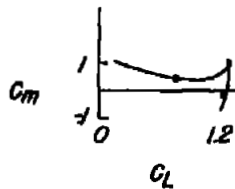


(f) $\alpha \approx 28.8^\circ$.

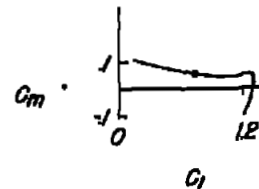
Figure 11.- Concluded.



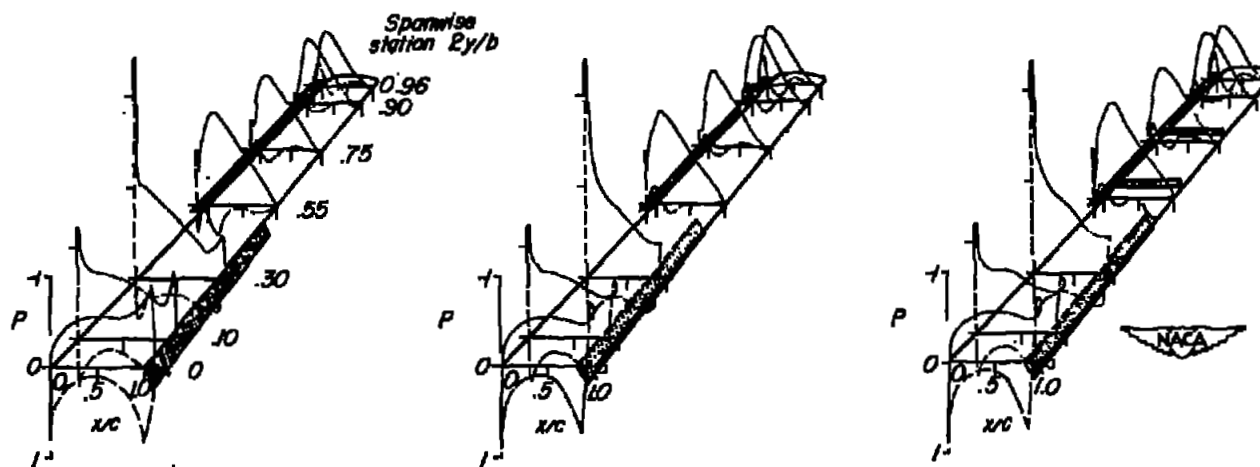
*0.5b/2 trailing-edge extended flaps
and 0.45b/2 leading-edge flaps*



*0.5b/2 trailing-edge split flaps
and 0.45b/2 leading-edge flaps*

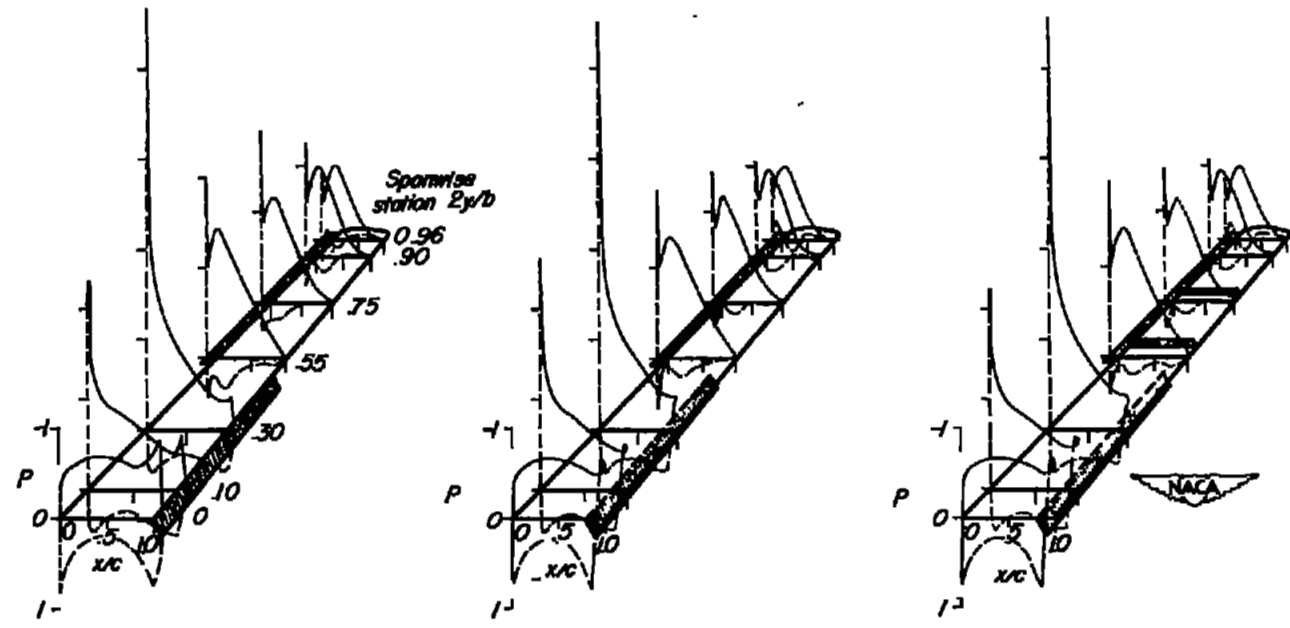
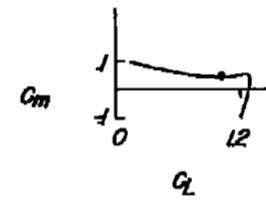
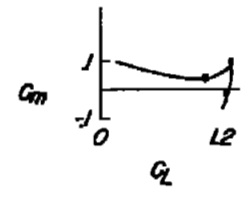
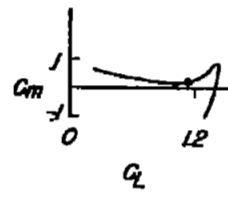


*0.5b/2 trailing-edge split flaps,
0.45b/2 leading-edge flaps
and upper-surface fences
at 0.575b/2 and 0.80b/2*



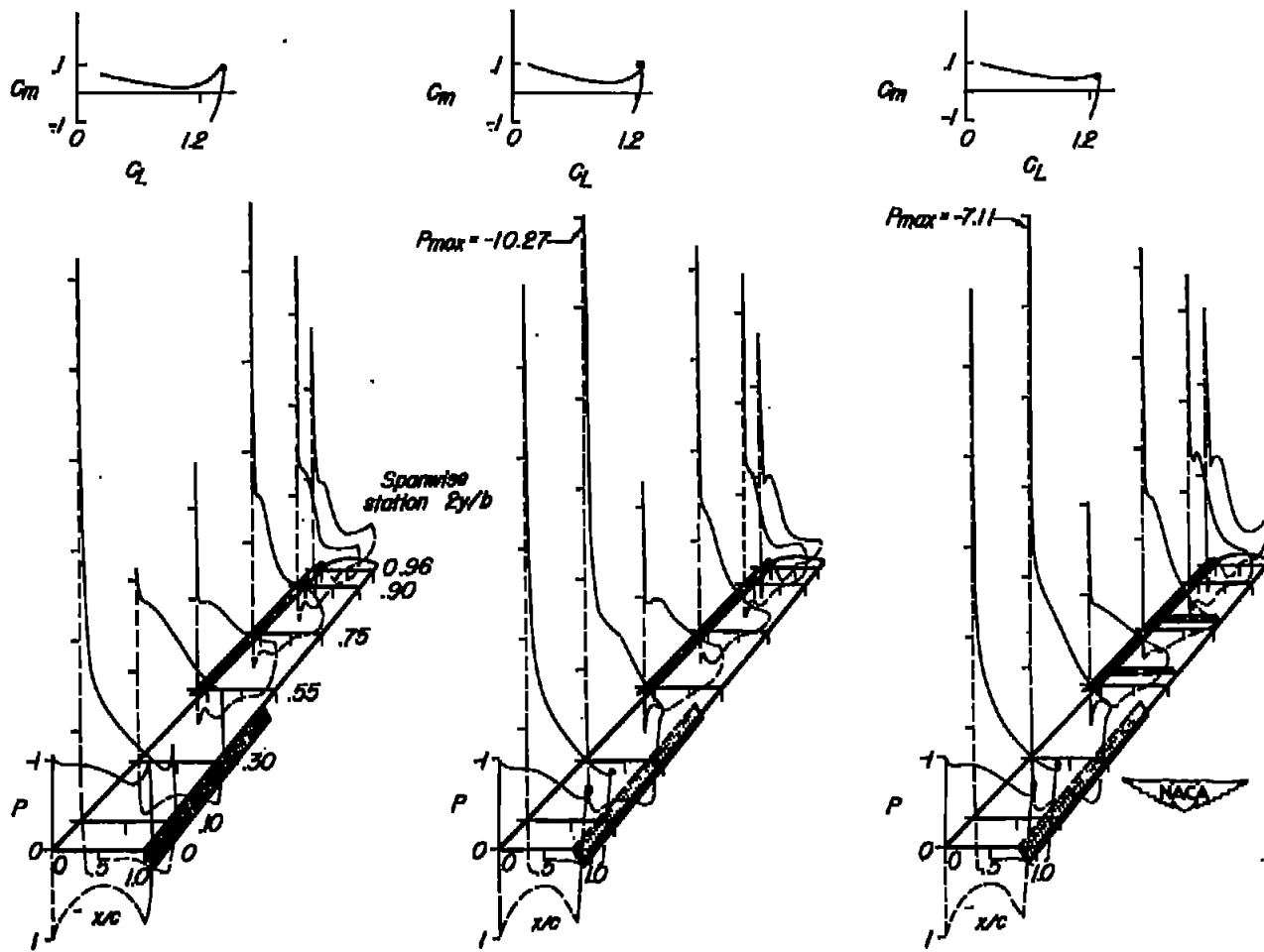
(a) $\alpha \approx 4.5^\circ$.

Figure 12.- Chordwise pressure distributions of wing with high-lift and stall-control devices deflected.



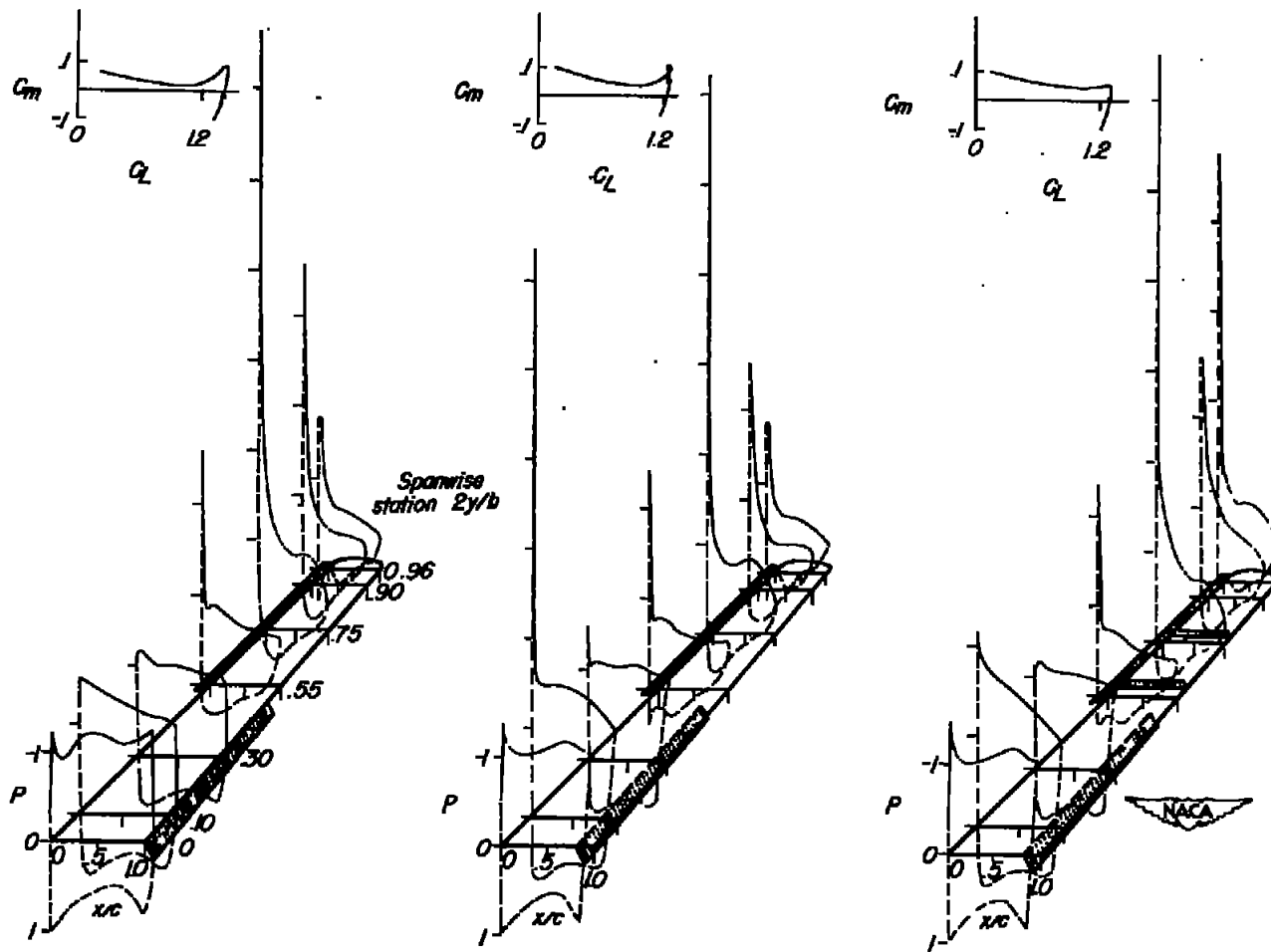
(b) $\alpha \approx 8.6^\circ$.

Figure 12.- Continued.



(c) $\alpha \approx 16.7^\circ$.

Figure 12.- Continued.



(d) $\alpha \approx 24.7^\circ$.

Figure 12.- Concluded.

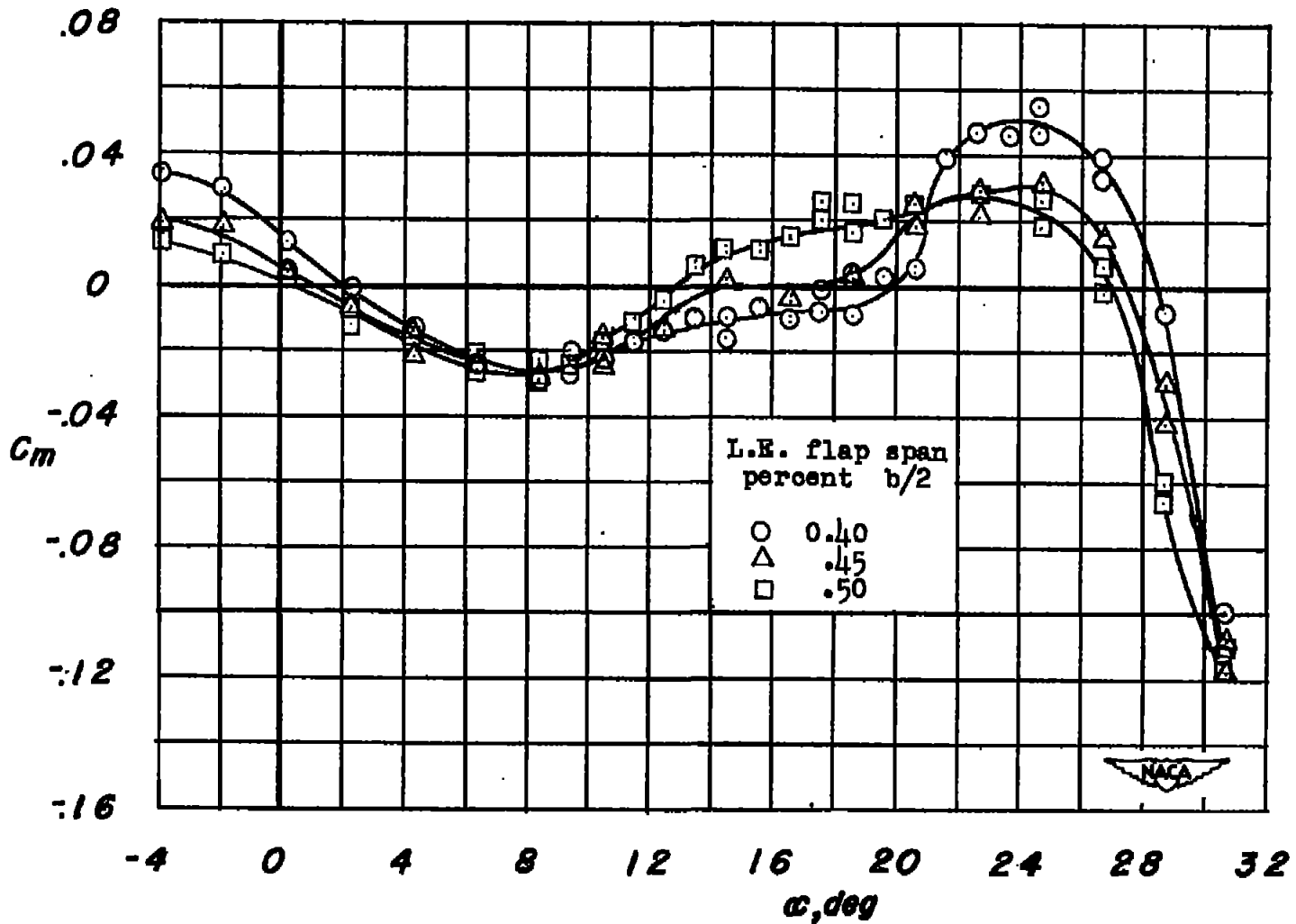


Figure 13.- Pitching-moment characteristics of the wing equipped with various spans of leading-edge flaps.

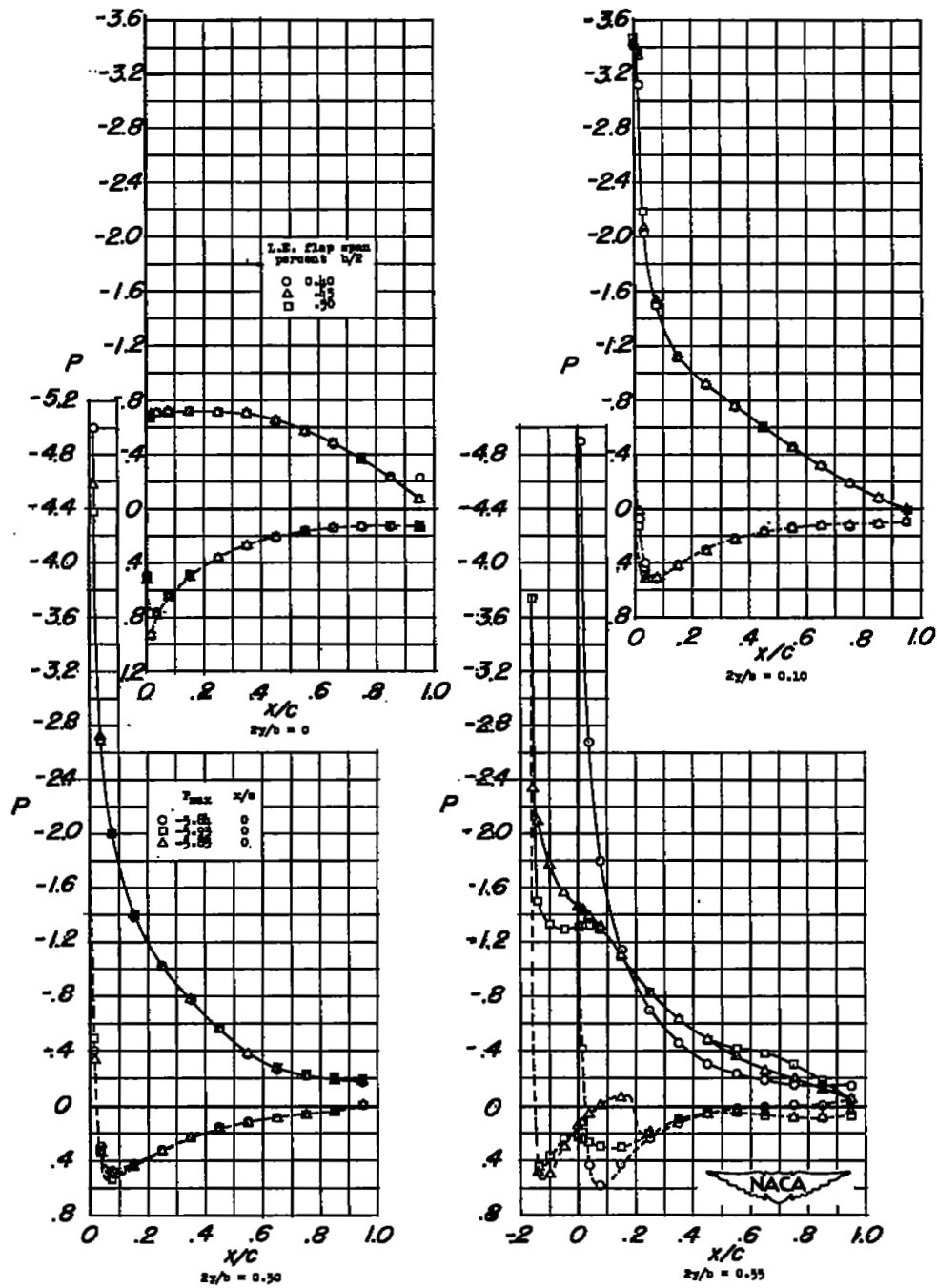
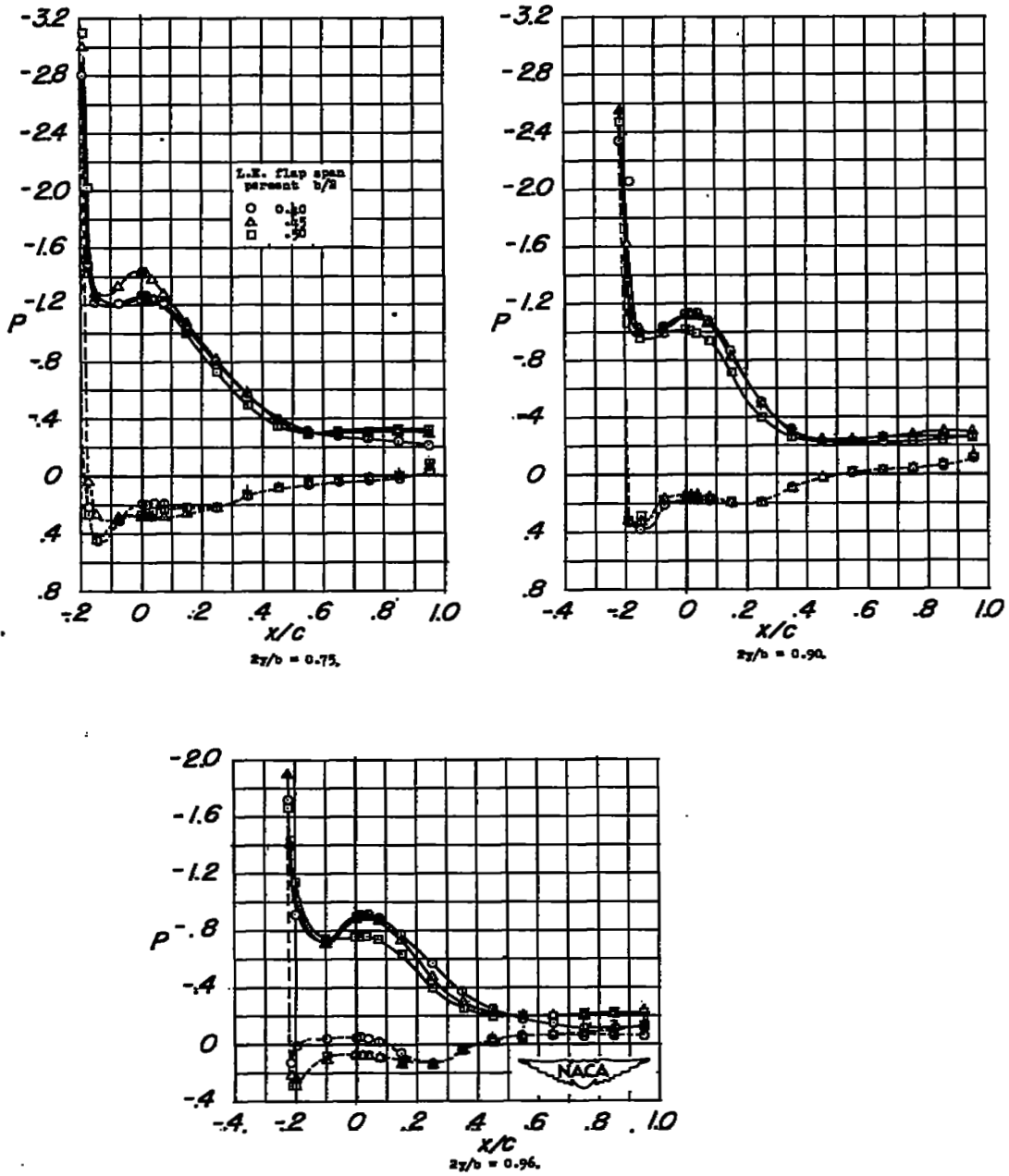
(a) $\alpha = 14.5^\circ$.

Figure 14.- Chordwise pressure distributions of the wing equipped with various spans of leading-edge flaps. Test points are taken from faired data.



(a) Concluded.

Figure 14.- Continued.

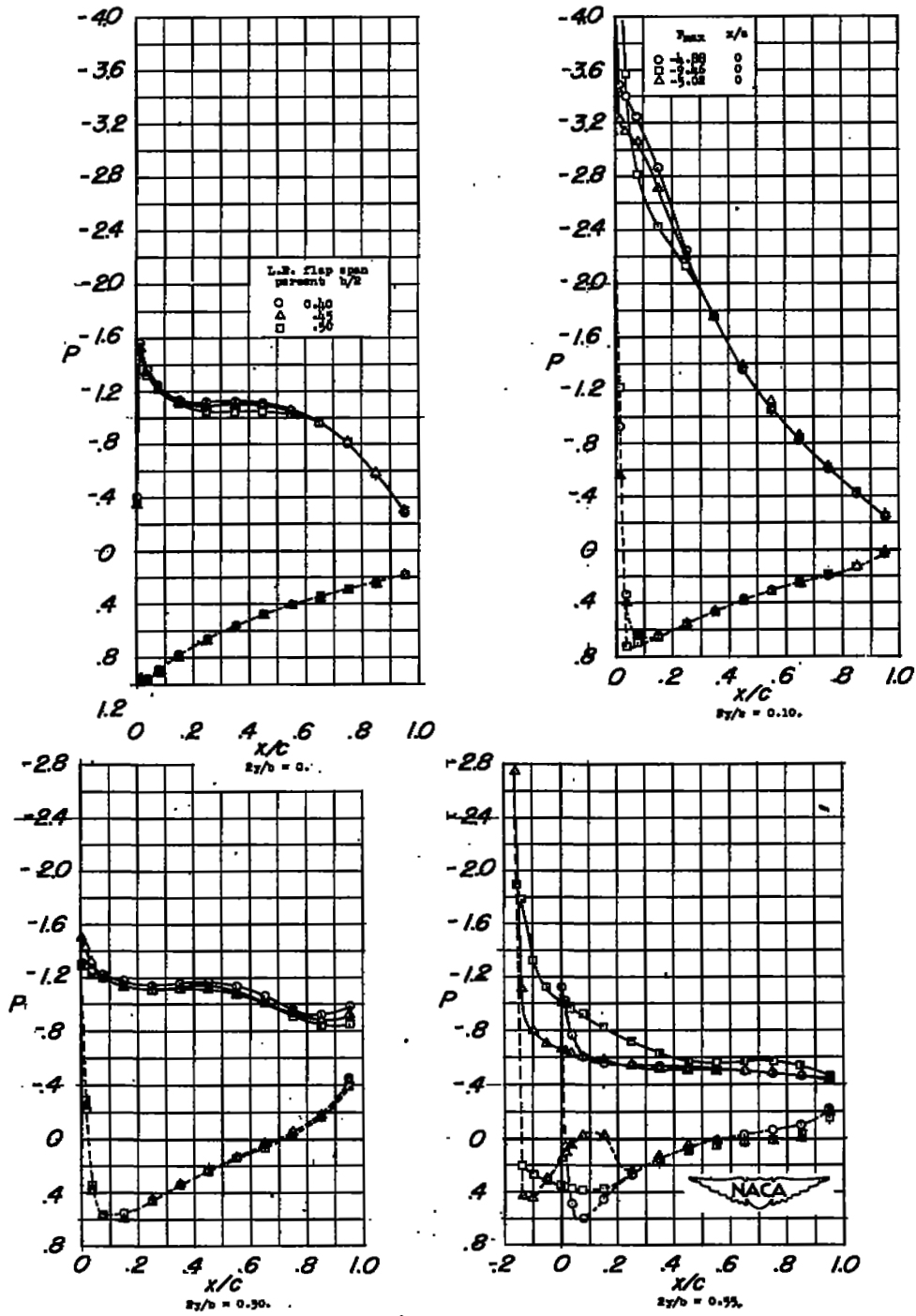
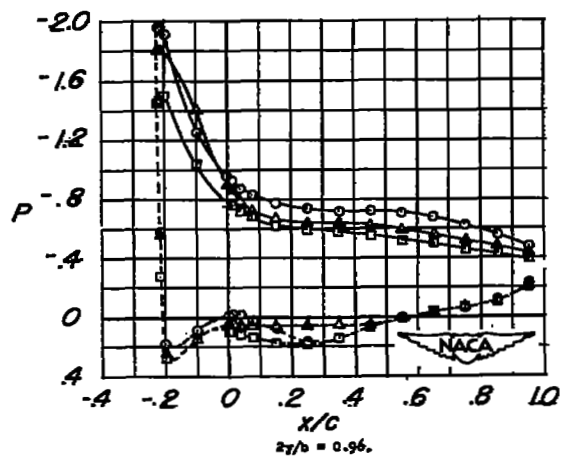
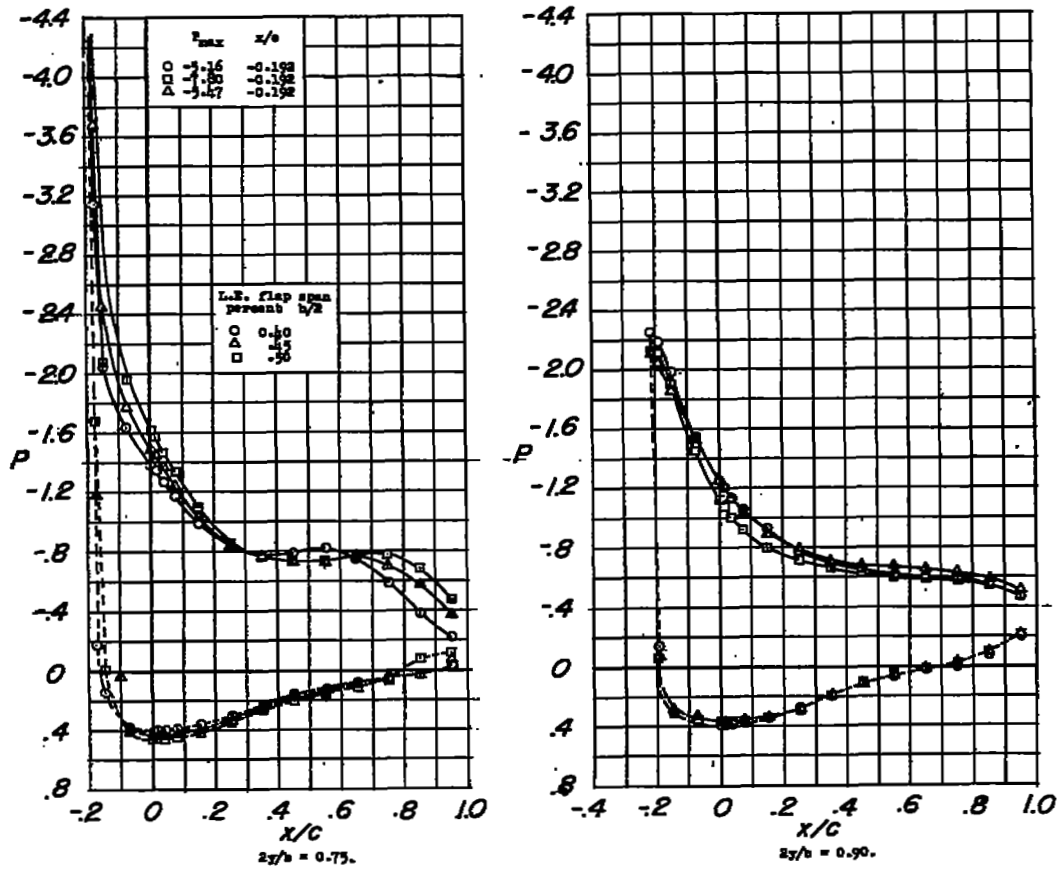
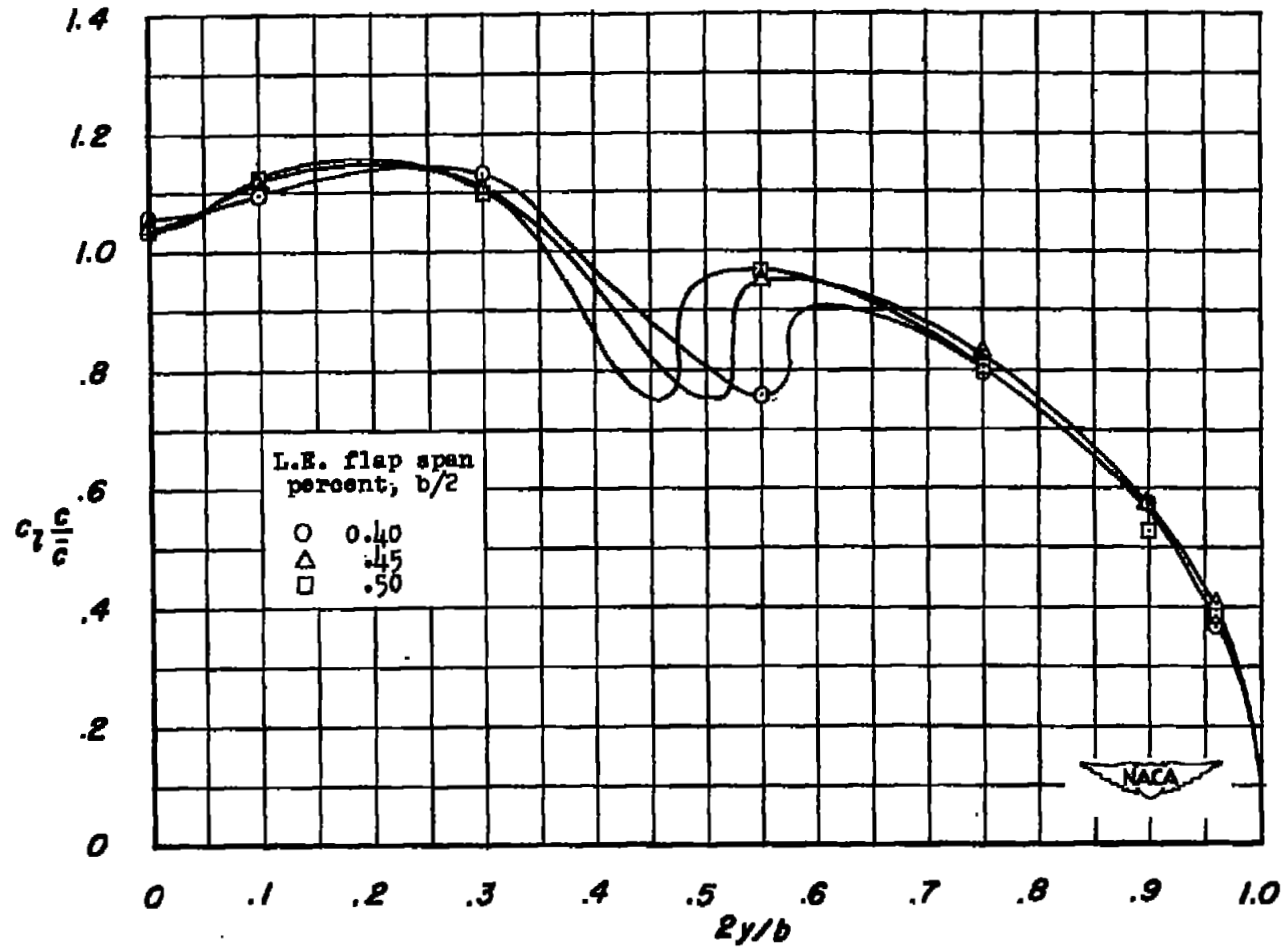
(b) $\alpha = 24.7^\circ$.

Figure 14.- Continued.



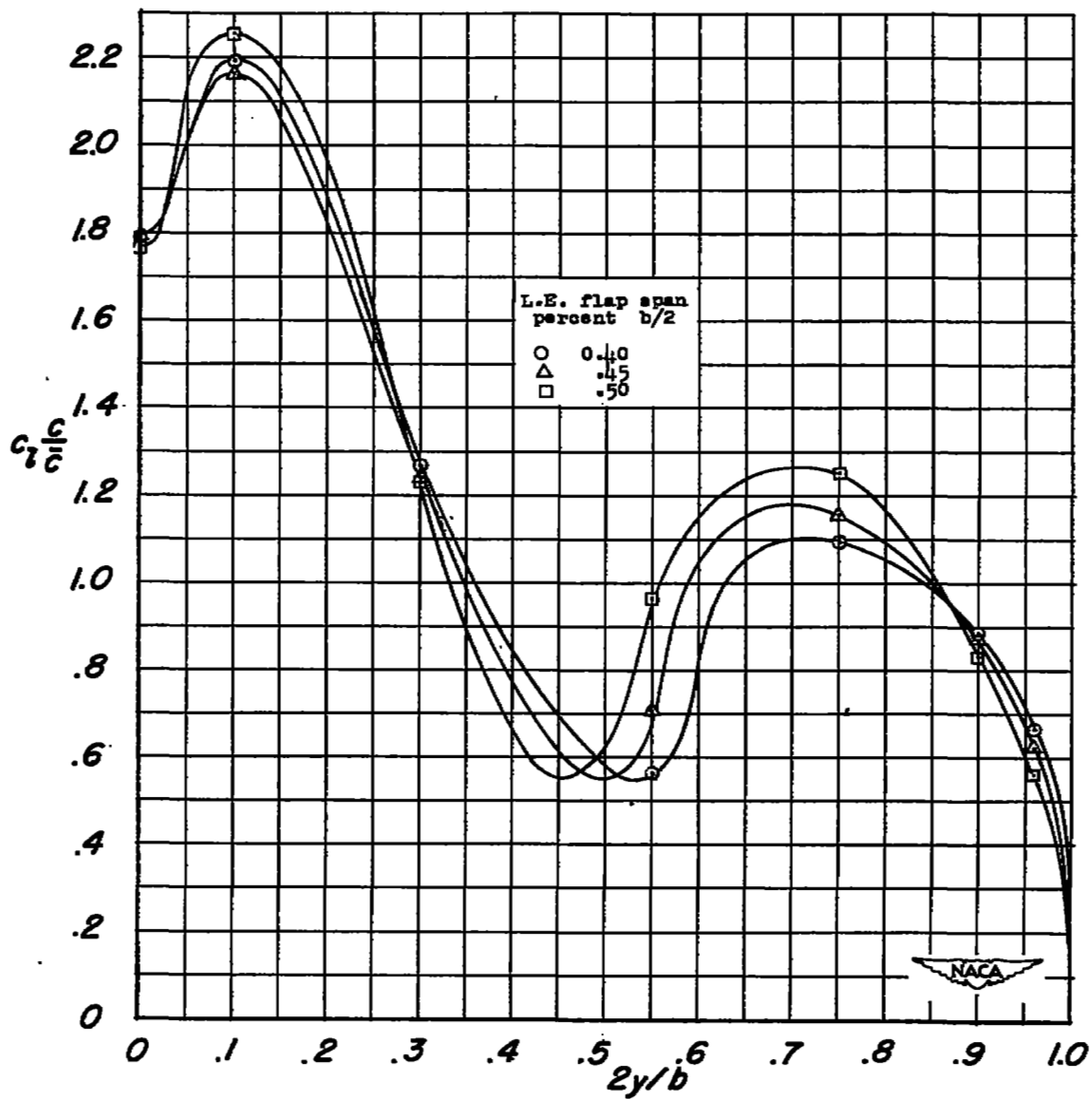
(b) Concluded.

Figure 14.- Concluded.



(a) $\alpha = 14.5^\circ$.

Figure 15.- Span load distributions of the wing equipped with various spans of leading-edge flaps.



(b) $\alpha = 24.7^\circ$.

Figure 15.- Concluded.

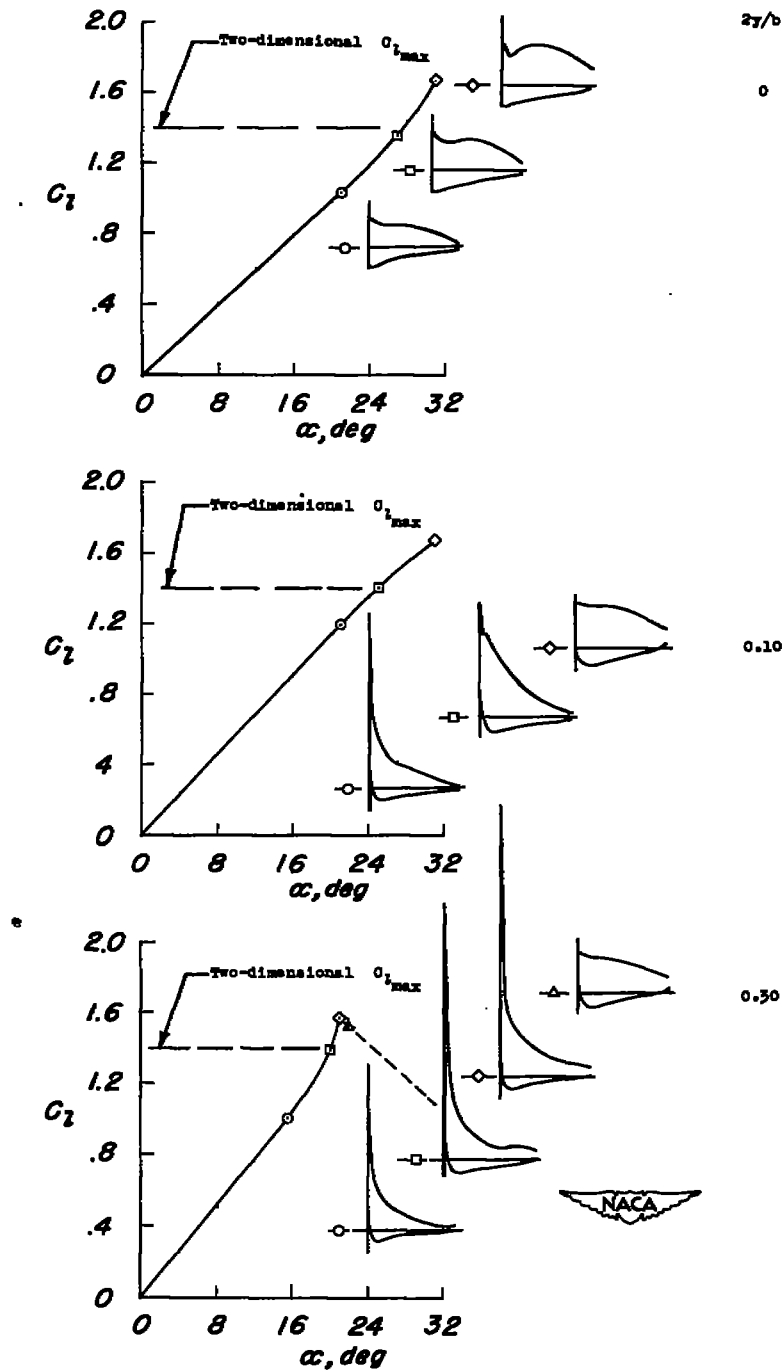


Figure 16.- Variation of section-lift coefficient and chordwise loadings with angle of attack for the spanwise stations $\frac{zy}{b} = 0, 0.10, \text{ and } 0.30$ (plain wing).

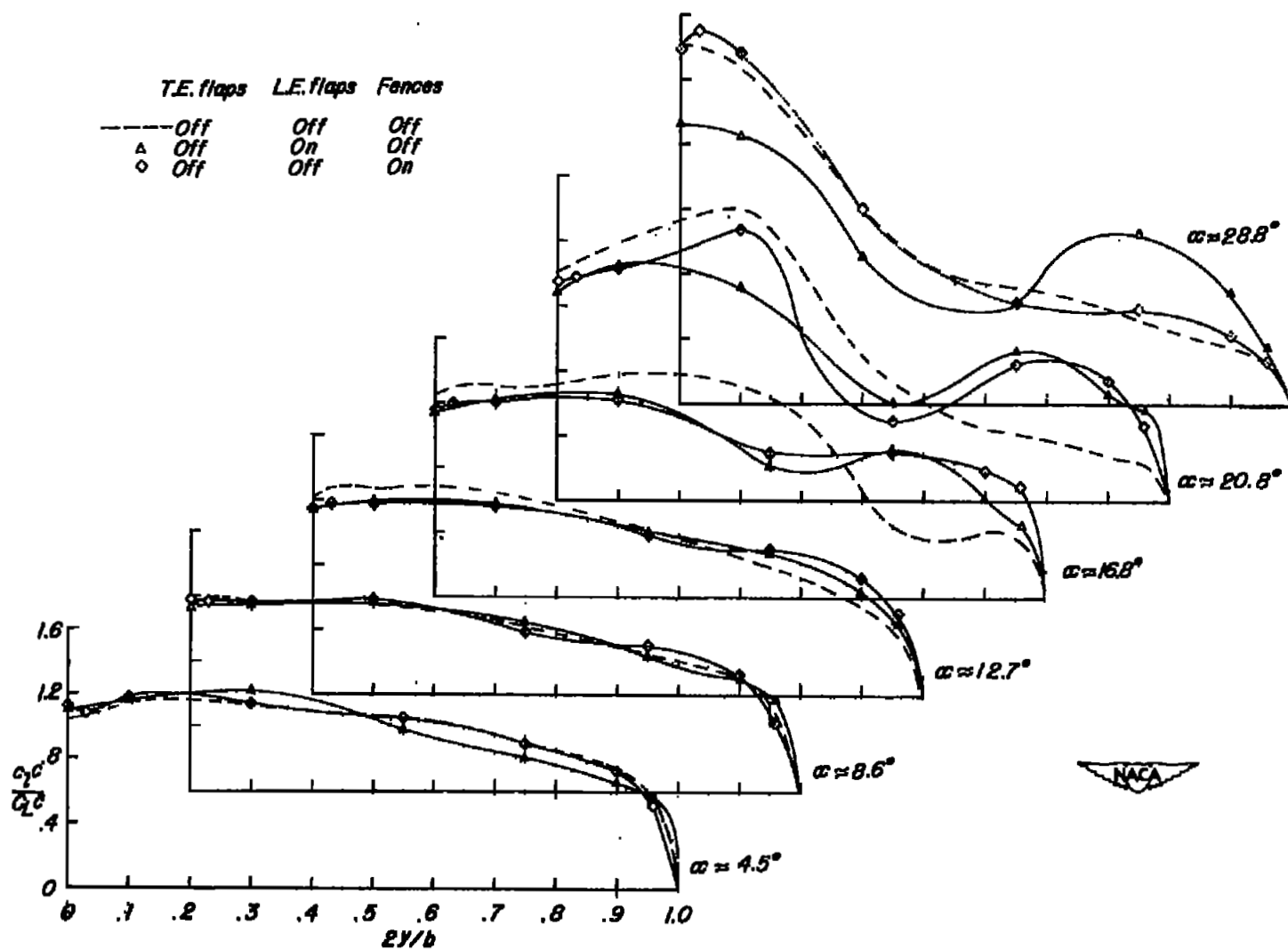


Figure 17.- Span-load distributions on the wing with and without stall-control devices installed.

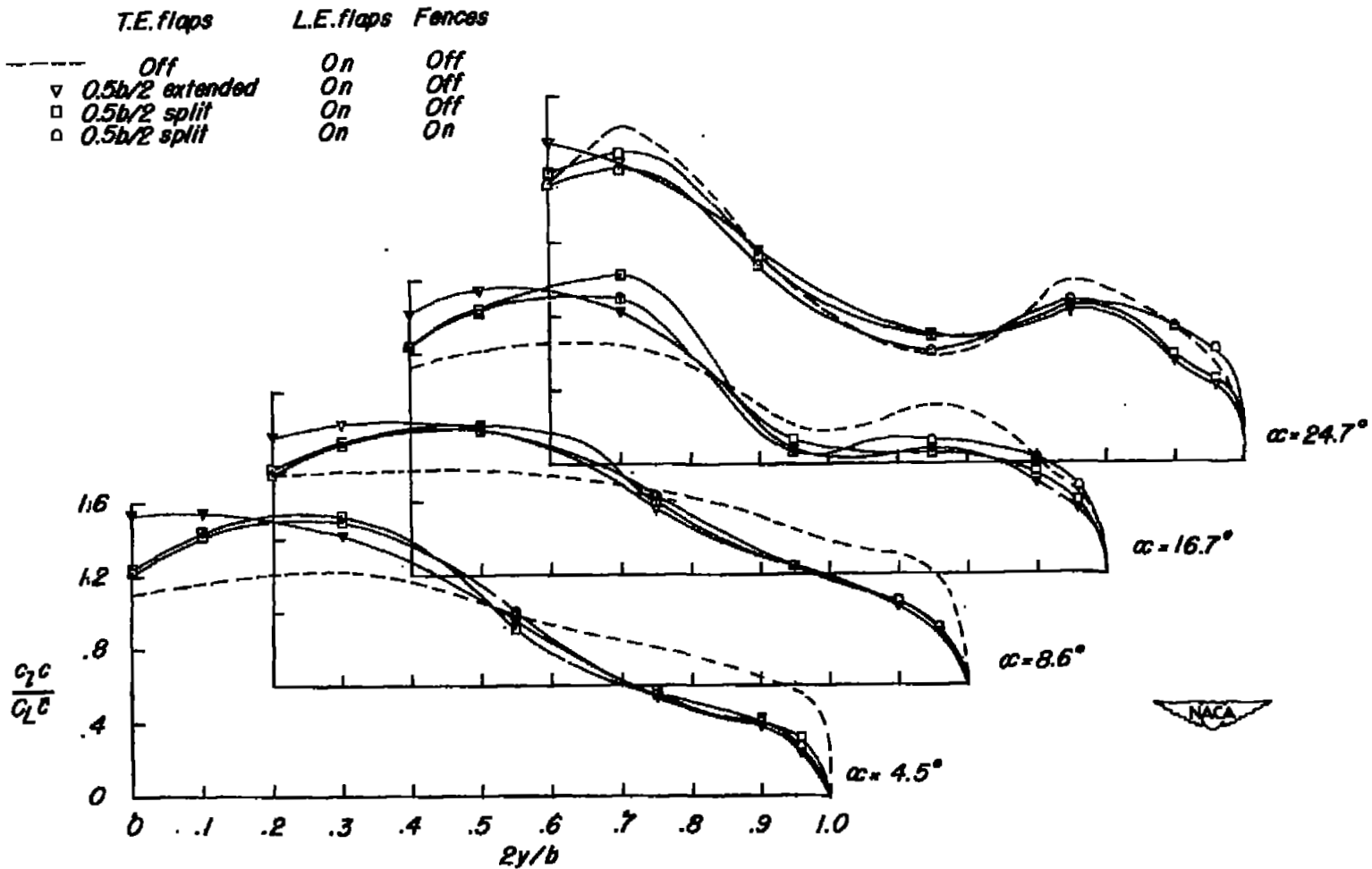


Figure 18.- Span-load distributions of the wing with high-lift and stall-control devices deflected.

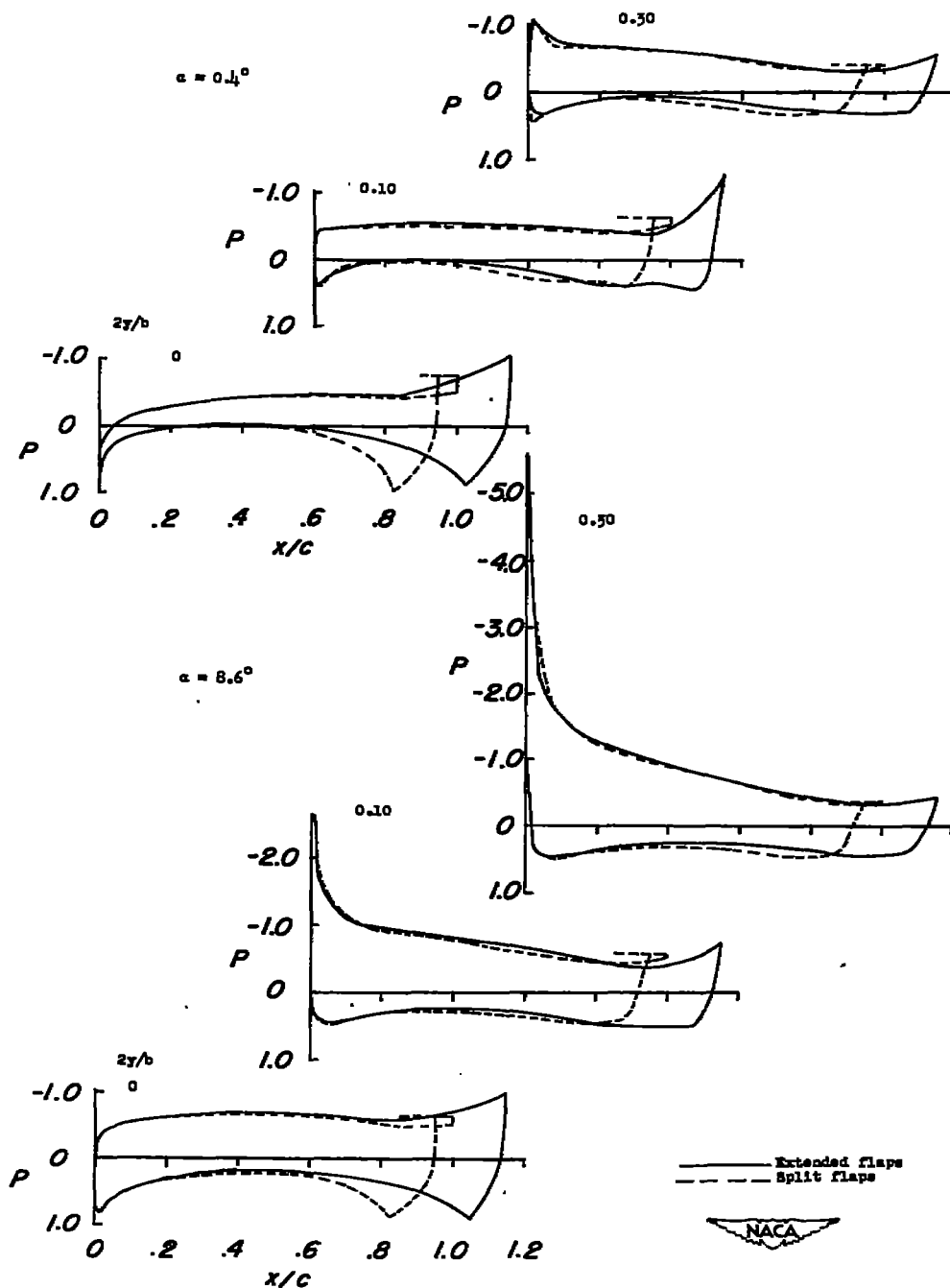
(a) $\alpha = 0.4^\circ$ and 8.6° .

Figure 19.- Chordwise pressure distributions of the inboard sections of the wing equipped with split and extended trailing-edge flaps. Wing equipped with $0.45b/2$ leading-edge flaps.

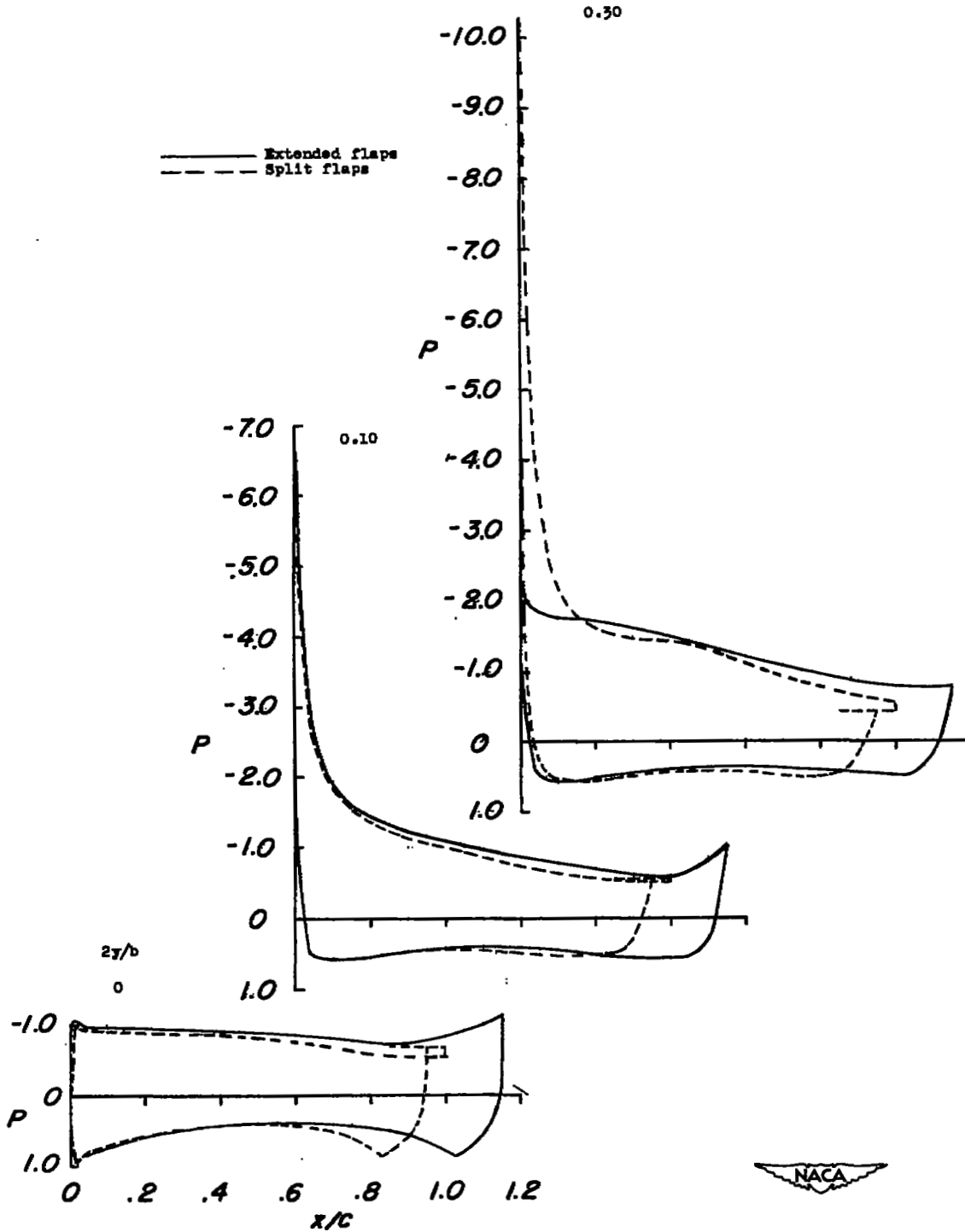
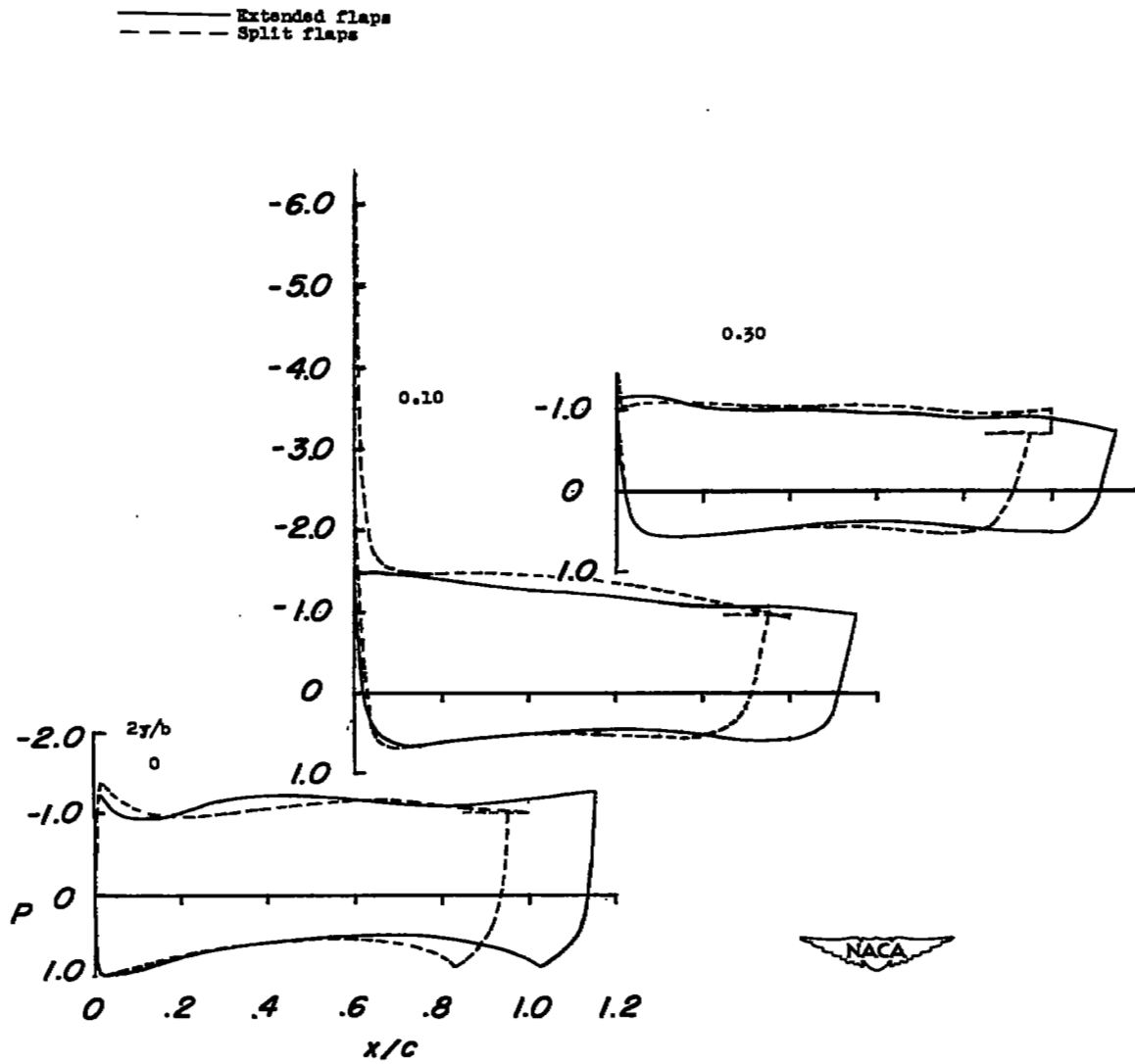
(b) $\alpha = 16.7^\circ$.

Figure 19.- Continued.



(c) $\alpha = 24.7^\circ$.

Figure 19.- Concluded.

SECURITY INFORMATION

NASA Technical Library



3 1176 01436 9772

